Training-Free Constrained Generation With Stable Diffusion Models

Stefano Zampini[*]
Polytechnic of Turin
stefano.zampini@polito.it

Jacob K. Christopher[*]
University of Virginia
csk4sr@virginia.edu

Luca Oneto
University of Genoa
luca.oneto@unige.it

Davide Anguita
University of Genoa
davide.anguita@unige.it

Ferdinando Fioretto[†]
University of Virginia
fioretto@virginia.edu

Abstract

Stable diffusion models represent the state-of-the-art in data synthesis across diverse domains and hold transformative potential for applications in science and engineering, e.g., by facilitating the discovery of novel solutions and simulating systems that are computationally intractable to model explicitly. While there is increasing effort to incorporate physics-based constraints into generative models, existing techniques are either limited in their applicability to latent diffusion frameworks or lack the capability to strictly enforce domain-specific constraints. To address this limitation this paper proposes a novel integration of stable diffusion models with constrained optimization frameworks, enabling the generation of outputs satisfying stringent physical and functional requirements. The effectiveness of this approach is demonstrated through material design experiments requiring adherence to precise morphometric properties, challenging inverse design tasks involving the generation of materials inducing specific stress-strain responses, and copyright-constrained content generation tasks. All code has been released at https://github.com/RAISELab-atUVA/Constrained-Stable-Diffusion.

1 Introduction

Diffusion models have emerged as powerful generative tools, synthesizing structured content from random noise through sequential denoising processes [1, 2]. These models have driven significant advancements across diverse domains, including engineering [3, 4], automation [5, 6], chemistry [7, 8], and medical analysis [9, 10]. The advent of stable diffusion models has further extended these capabilities, enabling efficient handling of high-dimensional data and more complex distributions [11]. This scalability makes stable diffusion models particularly promising for applications in science and engineering, where data is highly complex and fidelity is paramount.

However, despite their success in generating coherent content, diffusion models face a critical limitation when applied to domains that require outputs to adhere to strict criteria. In scientific and engineering contexts, generated data must go beyond merely resembling real-world examples; it must rigorously comply with predefined specifications, such as physical laws, safety standards, or design constraints grounded in first principles. When these criteria are not met, the outputs may become unreliable, unsuitable for practical use, or even hazardous, undermining trust in the model's applicability. *Bridging this gap is crucial for realizing the potential of diffusion models in scientific applications.*

[*] Equal contribution.
[†] Contact author

39th Conference on Neural Information Processing Systems (NeurIPS 2025).

Recent research has reported varying success in *augmenting model training* with (often specialized classes of) constraints and providing adherence to desired properties in selected domains [12–14]. Many of these methods, however, are restricted to simple constraint sets or feasible regions that can be easily approximated, such as a simplex, L2-ball, or polytope. These assumptions break down in scientific and engineering tasks where constraints may be non-linear, non-convex, or even non-differentiable. Others are fundamentally limited, as training-time enforcement offers only distribution-level adherence to constraints rather than per-sample guarantees, even in convex settings, and cannot generalize to unseen or altered constraints without retraining. While *inference-time* enforcement methods address these shortcomings, these approaches modify the reverse processes in the original data space [15, 16]. This makes them incompatible with diffusion models like Stable Diffusion, which operate on learned lower-dimensional representations of the data. Latent-space variants have begun to appear, but they rely on special measurement operators [17–19] or on learned soft penalties [20, 21], thus limiting general applicability to the problems of interest in this work.

We address this challenge by integrating a proximal mappings into the reverse steps of pretrained stable diffusion models. The paper makes the following contributions: At each iteration, the generated latent is adjusted with a gradient descent step on the score field followed by a proximal update for constraint correction, all without retraining the network. When the constraint set is convex we prove that every iterate remains in the feasible region and that the Markov chain converges almost surely to a feasible point. The same algorithm, kept unchanged, extends to strongly non-convex constraints and even to constraints that can be checked only through a black-box simulator by estimating stochastic subgradients with finite differences. Experiments on **(i)** porous-material synthesis with exact porosity and tortuosity, **(ii)** meta-material inverse design that matches target stress-strain curves through a finite-element solver in the loop, and **(iii)** content generation subject to copyright filters show near-zero violations and state-of-the-art performance in constrained generation.

2 Preliminaries: Diffusion Models

Score-Based Diffusion Models [22, 23] learn a data distribution by coupling a noising (forward) Markov chain with a learned denoising (reverse) chain. Let $\{\boldsymbol{x}_t\}_{t=0}^{T}$ be the sequence of diffusion states with $\boldsymbol{x}_0$ drawn from the original data distribution $p_{\text{data}}(\boldsymbol{x}_0)$. In the *forward process*, Gaussian noise is added according to a fixed variance schedule $\bar{\alpha}_t$, where $\bar{\alpha}_{t+1} \leq \bar{\alpha}_t$, so that the learned marginal $q(\boldsymbol{x}^T)$ approaches $\mathcal{N}(\boldsymbol{0}, \boldsymbol{I})$ as $t \to T$. A score network $s_\theta(\boldsymbol{x}_t, t)$ is trained to learn the score function $s_\theta(\boldsymbol{x}_t, t) = \nabla_{\boldsymbol{x}_t} \log q(\boldsymbol{x}_t|\boldsymbol{x}_0) \approx \nabla_{\boldsymbol{x}_t} \log p(\boldsymbol{x}_t|\boldsymbol{x}_0)$, where the approximation holds under the assumption that $q(\boldsymbol{x}_t|\boldsymbol{x}_0)$ is a close proxy for the true distribution $p(\boldsymbol{x}_t|\boldsymbol{x}_0)$. The network is trained by applying noise $\epsilon \sim \mathcal{N}(\boldsymbol{0}, \boldsymbol{I})$ perturbations to the $\boldsymbol{x}_0$, such that $\boldsymbol{x}_t = \sqrt{\bar{\alpha}_t}\boldsymbol{x}_0 + \sqrt{1-\bar{\alpha}_t}\epsilon$, with the training objective minimizing the predicted error in the score estimate of the noisy samples:

$$\min_{\theta} \mathop{\mathbb{E}}_{t\sim[1,T],\, \boldsymbol{x}_0\sim p_{\text{data}},\, \epsilon\sim\mathcal{N}(0,I)} \left[\| s_\theta(\boldsymbol{x}_t, t) - \nabla_{\boldsymbol{x}_t} \log q(\boldsymbol{x}_t \mid \boldsymbol{x}_0) \|_2^2 \right]. \tag{1}$$

In the *reverse process*, the trained score network $s_\theta(\boldsymbol{x}_t, t)$ is used to iteratively reconstruct data samples from the noise distribution $p(\boldsymbol{x}_T)$. At each step t, the model approximates the reverse transition, effectively reversing the diffusion process to *sample* high-quality data samples. Notably, Denoising Diffusion Probabilistic Models have been shown to be mathematically equivalent [2, 23].

Stable Diffusion. In latent-diffusion variants such as *Stable Diffusion* [24, 25], the same scheme operates in a compressed latent space. The architecture uses an encoder-decoder pair $\mathcal{E}$ and $\mathcal{D}$, where the encoder $\mathcal{E}$ maps the high-dimensional image data to a latent space, denoted $\mathbf{z}_t$, and the decoder $\mathcal{D}$ reconstructs the final image from the latent space after the diffusion model has operated on it. The training objective remains consistent with Equation (1), with the exception that noise is applied to $\mathbf{z}_0 = \mathcal{E}(\boldsymbol{x}_0)$ as opposed to directly to $\boldsymbol{x}_0$ as in ambient space diffusion models. The latent diffusion model is thus trained to denoise over the latent space as opposed to the image space. Notice, however, that training the denoiser does not directly interact with the decoder, as the denoiser's loss is defined over the latent space and does not connect to the finalized samples. This consideration is relevant to the design choice taken by this paper in the proposed solution, discussed in Section 4. After iterative denoising, the final sample can be obtained by decoding $\mathbf{z}_0$ with $\mathcal{D}$.

3 Projected Langevin Dynamics

Score-based diffusion models sample by running annealed Langevin dynamics, a form of Langevin Monte Carlo adapted to multiple noise levels. At each level t, one takes M iterations of

$$\boldsymbol{x}_t^{(i+1)} \;=\; \boldsymbol{x}_t^{(i)} + \gamma_t\, \boldsymbol{s}_\theta\big(\boldsymbol{x}_t^{(i)}, t\big) + \sqrt{2\gamma_t}\boldsymbol{\epsilon}, \quad \boldsymbol{\epsilon} \sim \mathcal{N}(\mathbf{0}, \boldsymbol{I}),$$

where $\boldsymbol{s}_\theta(\boldsymbol{x}, t) \approx \nabla_x \log q(\boldsymbol{x})$ is the fixed, learned score and γ_t is a step size. This update performs stochastic gradient ascent on the learned log-density $\log q(\boldsymbol{x})$ with added Gaussian noise [26]. This optimization is performed either directly [22] or as the corrector step within a predictor-corrector framework [23]; in both cases, the result is an approximate gradient ascent on the density function, subject to noise. Provided this understanding, Christopher et al. [15] showed that for a constraint set C, enforcing $\boldsymbol{x}_t^{(i+1)} \in \boldsymbol{C}$ turns sampling into a series of constrained problems.

Specifically, this framing shifts the traditional diffusion-based sampling procedure into a series of independent, per-timestep optimization subproblems, each responsible for denoising a single step while enforcing constraints:

$$\boldsymbol{x}_t^{(i+1)} = \mathcal{P}_{\mathbf{C}}\left(\boldsymbol{x}_t^{(i)} + \gamma_t \nabla_{\boldsymbol{x}_t^{(i)}} \log q(\boldsymbol{x}_t|\boldsymbol{x}_0) + \sqrt{2\gamma_t}\boldsymbol{\epsilon}\right), \tag{2}$$

where the projection operator $\mathcal{P}_{\mathbf{C}}(\boldsymbol{x}) = \mathrm{argmin}_{\boldsymbol{y}\in\mathbf{C}} \|\boldsymbol{y} - \boldsymbol{x}\|_2^2$ returns the nearest feasible sample. Note that Langevin dynamic annealing occurs in an external loop decreasing the noise level across $t = T, \ldots, 1$, so that noise level $\boldsymbol{\epsilon}$ and step size γ_t remain fixed inside each subproblem. As $t \to 0$ the noise vanishes and the Langevin dynamics converge to a deterministic gradient ascent on the learned density function. Note also that annealed Langevin dynamics is known to reach an ε-stationary point of the objective with high probability [27]. In diffusion processes, the negative learned density function, $-\log q(\boldsymbol{x}_t|\boldsymbol{x}_0)$, serves as the objective, so Equation (2) can be viewed as *projected gradient descent* on this landscape. The results of [27] extend to non-convex settings, giving further theoretical support to the constrained sampler adopted here.

While this approach is applicable when diffusion models operate across the image space, it cannot be directly adapted to the context of stable diffusion as $\mathbf{C}$ cannot be concretely represented in the latent space where the reverse process occurs. Other works have attempted to impose select criteria on latent representations, but these methods rely on learning-based approaches that struggle in out-of-distribution settings [20, 21], making them unsuitable for scenarios requiring strict constraint adherence. This limitation likely explains their inapplicability in the engineering and scientific applications explored by [13–15].

4 Latent Space Correction

Addressing the challenge of imposing constraints directly in the latent space hinges on a key insight: while constraints may not be representable in the latent domain, their satisfaction can be evaluated at any stage of the diffusion process. Indeed, the decoder, $\mathcal{D}$, facilitates provides a differentiable transformation from the latent representation to the image space, where constraint violations can be directly quantified. Therefore, when the constraint function is differentiable, or even if its violations can be measured via a differentiable mechanism, gradient-based methods can be used to iteratively adjust the latent representation throughout the diffusion process to ensure constraint adherence.

4.1 Imposing Ambient Space Constraints on the Latent

This section begins by describing how constraints defined in the ambient space can be imposed on the latent during the denoising process. First, following the constrained optimization framework discussed in Section 3, at each noise level t we recast the reverse process for *Stable Diffusion* as the following constrained optimization problem:

$$\underset{\mathbf{z}_T,\ldots,\mathbf{z}_1}{\text{minimize}} \sum_{t=T,\ldots,1} -\log q(\mathbf{z}_t|\mathbf{z}_0) \qquad \text{s.t.:} \quad \mathbf{g}(\mathcal{D}(\mathbf{z}_t)) = 0, \tag{3}$$

where $\mathcal{D}$ maps the latent representation $\mathbf{z}_t$ into its original dimensions and $\mathbf{g}$ is a differentiable vector-valued function $\mathbf{g} : \mathbb{R}^d \to [0, \infty]$ measuring the distance to the constraint set $\mathbf{C}$. At each iteration of the diffusion process, our goal is to restore feasibility with respect to $\mathbf{g}$.

As the constraint function can only be meaningfully represented in the image space, its gradients with respect to the latent variables are computed by evaluating the function on the decoded representation $\mathcal{D}(\mathbf{z}_t)$. This process is facilitated by the computational graph:

$$\mathbf{z}_t \leftarrow \mathcal{D}(\mathbf{z}_t) = \boldsymbol{x}_t \leftarrow \mathbf{g}(\boldsymbol{x}_t) = \inf_{\boldsymbol{y} \in \mathbf{C}} \|\boldsymbol{y} - \boldsymbol{x}_t\|. \tag{4}$$

This enables iterative updates that reduce constraint violations by backpropagating gradients from the constraint function directly to the latent representation as,

$$\nabla_{\mathbf{z}_t} \mathbf{g} = \big(\partial \mathcal{D} / \partial \mathbf{z}_t\big)^\top \nabla_{\boldsymbol{x}_t} \mathbf{g}.$$

Thus constraint information, computed where it is meaningful (image space), can be back-propagated through the frozen decoder to steer the latent variables. The method leaves the score network and the decoder unchanged, adds no learnable parameters, and enables feasibility enforcement at every step even when $\boldsymbol{C}$ is non-convex or specified only by a black-box simulator.

4.2 Proximal Langevin Dynamics

The representation of latent diffusion as a constrained optimization task enables the application of established techniques from constrained optimization. To this end, this section discusses a generalization of the orthogonal projections used in projected Langevin dynamics, formulated through a *Proximal Langevin Dynamics* scheme. Let a constraint be encoded by a proper, lower-semicontinuous convex penalty $\mathbf{g} : \mathbb{R}^d \to [0, \infty]$ whose zero set coincides with the feasible region. After each noisy ascent step we apply a proximal map:

$$\boldsymbol{x}_t^{(i+1)} = \text{prox}_{\lambda \mathbf{g}} \underbrace{\Big(\boldsymbol{x}_t^{(i)} + \gamma_t \nabla_{\mathbf{z}_t^{(i)}} \log q(\boldsymbol{x}_t | \boldsymbol{x}_0) + \sqrt{2\gamma_t}\boldsymbol{\epsilon}\Big)}_{\text{Langevin Dynamics Step}}, \tag{5}$$

with the proximal operator defined as:

$$\text{prox}_{\lambda \mathbf{g}}(\boldsymbol{x}_t) = \arg\min_{\boldsymbol{y}} \big\{\mathbf{g}(\boldsymbol{y}) + \tfrac{1}{2\lambda}\|\boldsymbol{y} - \boldsymbol{x}_t\|_2^2\big\}. \tag{6}$$

This operator balances maintaining similarity to the updated sample and adhering to the constraint function $\mathbf{g}$ as weighted by hyperparameter λ. Choosing $\mathbf{g}$ as the indicator of a set, reproduces the familiar projection step introduced earlier, but the proposed Proximal Langevin Dynamics also accommodates non-smooth regularizers, composite penalties, and constraints specified only through inner optimization subroutines [28–30]. Thus, because proximal maps can be evaluated efficiently even for implicit or geometrically intricate constraints, Proximal Langevin Dynamics extends Langevin-based sampling to settings where explicit projections are impractical while preserving the convergence guarantees of the original scheme. The next results provides a characterization on convergence to **(i)** the constraint set and **(ii)** the original data distribution p_{data}.

Theorem 4.1 (Convergence to the Constraint Set)**.** *Let $\boldsymbol{C}$ be non-empty and β-prox-regular in the sense of [31], Def. 13.27, the score network satisfy $\|\nabla_{\boldsymbol{x}_t} \log q(\boldsymbol{x}_t)\| \leq G$ (a standard consequence of the bounded-data domain after normalization), and $\mathcal{D}$ is ℓ-Lipschitz such that $\|\nabla \mathcal{D}(\mathbf{z})\| \leq \ell$. Then, for positive step sizes $\gamma_t, \leq \frac{1}{2G^2}\beta$, the following inequality holds for the distance to $\boldsymbol{C}$:*

$$\text{dist}\big(\mathcal{D}(\mathbf{z}'_t), \boldsymbol{C}\big)^2 \;\leq\; (1 - 2\beta'\gamma_{t+1})\ \text{dist}\big(\mathcal{D}(\mathbf{z}'_{t+1}), \boldsymbol{C}\big)^2 + \gamma_{t+1}^2 G^2, \quad \text{(non-asymptotic feasibility)}$$

where $\mathbf{z}'_t$ is the pre-proximal mapping iterate, g is L-smooth, $\beta' = \beta/(\ell L)$, and $\text{dist}(\mathbf{z}'_t, \boldsymbol{C})$ is the distance from $\mathbf{z}'_t$ to the feasible set $\boldsymbol{C}$.

Theorem 4.1 illustrates that the distance to the feasible set $\boldsymbol{C}$ decreases at a rate of $1 - 2\beta'\gamma_{t+1}$ at each step (up to an additive $\gamma_{t+1}^2 G^2$ noise). Thus, the iterates converge to an ϵ-feasible set in $\mathcal{O}(\frac{1}{\gamma_{\min}} \log(\frac{1}{\varepsilon}))$ steps, with $\gamma_{\min} = \min_t \gamma_t$. This is experimentally reflected in Section 6.1, where $\mathbf{C}$ is convex and *all samples* converge to the feasible set.

Theorem 4.2 (Training Distribution Fidelity)**.** *Suppose the assumptions stated in Theorem 4.2 are satisfied. Then, for positive step sizes $\gamma_t, \leq \frac{1}{2G^2}\beta$, the following inequality holds for the Kullback-Leibler (KL) divergence from the data distribution:*

$$\text{KL}\big(q(\mathbf{z}_{t-1}) \,\|\, p_{\text{data}}\big) \leq \text{KL}\big(q(\mathbf{z}_t) \| p_{\text{data}}\big) + \gamma_t G^2, \quad \text{(fidelity)}$$

The inequality in Theorem 4.2 shows that the divergence from the training data distribution increases by at most $\frac{\beta}{2}$ (since $\gamma \leq \frac{1}{2G^2}\beta$) at each step and, consequently the cumulative divergence from the training distribution is $\mathcal{O}(\sum_t \gamma_t)$ and thus vanishes as $t \to 0$. Consequently, after at most $T^\star = \lceil \frac{1}{2\beta\gamma_{\min}} \log\big(\frac{\operatorname{dist}(x_T, \boldsymbol{C})^2}{\varepsilon}\big) \rceil$ steps the expected constraint violation drops below ε while their KL divergence from the original data distribution grows at most linearly in $\sum_t \gamma_t$ (negligible because $\gamma_t \to 0$ along the chain). This implies that our approach inherits the *same* sample quality guarantees as unconstrained diffusion, up to a tunable drift bounded by $\gamma_{\max} G^2$, (with $\gamma_{\max} = \max_t \gamma_t$), and, since $\gamma_t \to 0$ along the chain, this drift is negligible in practice. This result provides theoretical rationale for our method's comparable FID scores to unconstrained baselines for the image generation tasks in Sections 6.1 and 6.3. Proofs for both theorems are provided in Appendix H.

4.3 Training-Free Correction Algorithm

With the theoretical framework of our approach established, we are now ready to formalize the proposed training-free algorithm to impose constraints on $\mathbf{z}_t$. The algorithm can be decomposed into an outer minimizer, which corrects $\mathbf{z}_t$ throughout the sampling process, and an inner minimizer, which solves the proximal mapping subproblem. The former describes a high-level view of the entire constrained sampling process, whereas the latter presents the single-step sub-optimization procedure.

Outer minimizer. First, to impose corrections throughout the latent denoising process Equation (6) is modified to accommodate the $\mathcal{D}$ mapping:

$$\operatorname{prox}_{\lambda \mathbf{g}}(\mathbf{z_t}) = \arg\min_{\boldsymbol{y}} \left\{ \mathbf{g}(\mathcal{D}(\boldsymbol{y})) + \tfrac{1}{2\lambda} \|\mathcal{D}(\boldsymbol{y}) - \mathcal{D}(\mathbf{z_t})\|_2^2 \right\} \tag{7}$$

At each sampling iteration, we first compute the pre-projection update $\mathbf{z}_t' = \mathbf{z}_t + \gamma_t \nabla_{\mathbf{z}_t} \log q(\mathbf{z}_t|\mathbf{z}_0) + \sqrt{2\gamma_t}\boldsymbol{\epsilon}$ which incorporates both gradient and stochastic noise terms. We then apply a proximal operator to obtain the corrected latent $\hat{\mathbf{z}}_t = \operatorname{prox}_{\lambda \mathbf{g}}(\mathbf{z_t}')$. This follows the Proximal Langevin Dynamics scheme outlined in the previous section.

Inner minimizer. Each proximal mapping is composed of a series of gradient updates to solve the outer minimizer. In practice, gradient descent is applied on the proximal operator's objective:

$$\mathbf{z}_t^{i+1} = \mathbf{z}_t^i - \nabla_{\mathbf{z}_t^i} \left[\mathbf{g}(\mathcal{D}(\mathbf{z}_t^i)) + \tfrac{1}{2\lambda} \|\mathcal{D}(\mathbf{z}_t^i) - \mathcal{D}(\mathbf{z_t^0})\|_2^2 \right].$$

When a convergence criterion is met (e.g., $\mathbf{g}(\mathcal{D})(\mathbf{z}_t^{(i)}) < \delta$), the algorithm proceeds to the next denoising step. Algorithm 1 provides a pseudo-code for this gradient-based approach to applying the proximal operator within the stable diffusion sampling process.

In the case that $\mathbf{g}$ is an indicator function,

$$\mathbf{g}(\boldsymbol{y}) = \begin{cases} 0, & \boldsymbol{y} \in \mathbf{C}, \\ \infty, & \boldsymbol{y} \notin \mathbf{C}, \end{cases}$$

the proximal mapping reduces to a projection onto the constraint set. If $\mathcal{P}_\mathbf{C}$ can be formulated in the ambient space, the minimization can be fully imposed on the projection objective, $\|\mathcal{P}_\mathbf{C}(\mathcal{D}(\mathbf{z}_t)) - \mathcal{D}(\mathbf{z}_t)\|_2^2$. Notably, the gradients of this objective capture both the constraint violation term, $\mathbf{g}(\mathcal{D}(\mathbf{z}_t))$, and the distance term, $\frac{1}{2\lambda}\|\mathcal{D}(\boldsymbol{y}) - \mathcal{D}(\mathbf{z_t})\|_2^2$, within the prescribed tolerance, resulting in the solution to Eq. (7) at the end of the minimization. When $\mathbf{C}$ is convex, the projection can be constructed in closed-form (Section 6.1), but otherwise a Lagrangian relaxation can be employed [32]. For our experiments with non-convex constraint sets (Sections 6.2 and 6.3), we leverage an Augmented Lagrangian relaxation as described in Appendix D [33].

Algorithm 1: Sampler with Constraint Correction

```
Input: $\delta$ (violation tolerance), lr (learning rate)
Define prox_objective($\boldsymbol{x}_t^i$):
    violation ← $\mathbf{g}(\boldsymbol{x}_t^i)$;
    distance ← $\frac{1}{2\lambda}\|\boldsymbol{x}_t^i - \boldsymbol{x}_t^0\|_2^2$;
    return violation + distance;
for $t \leftarrow T$ to 0 do
    // Sampling steps (omitted).
    $i \leftarrow 0$;
    while $\mathbf{g}(\mathcal{D}(\mathbf{z}_t^i)) \geq \delta$ do
        $g \leftarrow \nabla_{\mathbf{z}_t^i}$prox_objective$(\mathcal{D}(\mathbf{z}_t^i))$;
        $\mathbf{z}_t^{i+1} \leftarrow \mathbf{z}_t^i - (g \times \text{lr})$;  $i \leftarrow i + 1$;
Output: $\mathcal{D}(\mathbf{z}_0)$
```

Importantly, in these cases the corrective step can be considered a projection of the latent under appropriate smoothness assumptions. We justify this claim with the following rationale: under the assumption of latent space smoothness [34], the nearest feasible point in the image space closely corresponds to the nearest feasible point in the latent space. Therefore, while the distance component of the proximal operator, $\frac{1}{2\lambda}\|\mathcal{D}(\mathbf{z}_t^i) - \mathcal{D}(\mathbf{z}_\mathbf{t}^\mathbf{0})\|_2^2$, is evaluated in the image space, minimizing this distance in the image space also minimizes the corresponding distance in the latent space, validating the use of this corrective step as a latent projector.

Finally, when $\mathbf{g}$ cannot be represented by a differentiable function, such as when the constraints are evaluated by an external simulator (as in Section 6.2) or when the constraints are too general to represent in closed-form (as in Section 6.3), it is necessary to approximate this objective to Equation (7) using other approaches. We discuss this further in the next section and empirically validate such approaches in Section 6.

5 Complex Constraint Evaluation

While in the previous section we discuss how to endow mathematical properties within stable diffusion, many desirable properties cannot be directly expressed as explicit mathematical expressions. Particularly when dealing with physical simulators, heuristic-based analytics, and partial differential equations, it becomes often necessary to either **(i)** estimate these constraints with surrogate models or **(ii)** approximate the gradients of black-box models. To this end, we propose two proxy constraint correction methods that leverage differentiable optimization to enforce constraints.

Differentiable surrogates. Surrogate models introduce the ability to impose soft constraints that would otherwise be intractable. Specifically, we replace $\mathbf{g}(\boldsymbol{x}_t)$, the constraint evaluation function used in the optimization process, with a constraint violation function dependent on the surrogate model (e.g., a distance function between the target properties and the surrogate model's predictions for these properties in $\boldsymbol{x}_t$ as shown in Section 6.3). This allows the surrogate to directly evaluate and guide the samples to adhere to the desired constraints at each step. Apart from this substitution, the overall algorithm remains identical to Algorithm 1. Through iterative corrections, the model *converges* to a corrected sample $\hat{\mathbf{z}}_t$ that satisfies the target constraints to the extent permitted by the surrogate's predictive accuracy. Appendix C provides an in-depth view of the differences of this approach with respect to classifier guidance.

Differentiating through black-box simulators. In some cases (including the setting of our metamaterial design experiments in Section 6.2), a strong surrogate model cannot be leveraged to derive accurate violation functions. In such settings, the only viable option is to use a simulator to evaluate the constraints. However, these simulators are often non-differentiable, making it impossible to directly compute gradients for the proximal operator. To incorporate the non-differentiable simulator into the inner minimization process, this paper exploits a sensitivity analysis method inspired by the *differentiable perturbed optimizer (DPO)* adopted in the context of differentiable optimization [35, 36]. DPO introduces controlled perturbations to the optimization variables and smooths the resulting objective, yielding differentiable surrogate gradients. Following this idea, random local perturbations are injected into the simulator inputs and define a smoothed function $\bar{\phi}_\nu(\boldsymbol{x}_t) = \mathbb{E}_\epsilon[\phi(\boldsymbol{x}_t + \nu\epsilon)]$, where ϕ is the external simulator, $\epsilon \sim \mathcal{N}(0, I)$ is a random perturbation, and ν is a temperature parameter controlling the smoothing scale. An unbiased Monte Carlo estimate of $\bar{\phi}_\epsilon$ is obtained as

$$\bar{\phi}_\epsilon(\boldsymbol{x}_t) = \frac{1}{M}\sum_{m=1}^{M} \phi\Big(\boldsymbol{x}_t + \nu\epsilon^{(m)}\Big),$$

where M is the number of perturbed samples. The gradient of this smoothed objective can be written as

$$\nabla_{\boldsymbol{x}_t}\bar{\phi}_\nu(\boldsymbol{x}_t) = \frac{1}{\nu}\,\mathbb{E}[\phi(\boldsymbol{x}_t + \nu\epsilon)\,\epsilon],$$

which corresponds to a finite-difference estimator whose scaling term $1/\nu$ is absorbed into the proximal step size during optimization. Finally, this smoothed estimator enables a differentiable loss formulation:

$$\nabla_{\boldsymbol{x}_t}\mathcal{L}(\phi(\boldsymbol{x}_t)) = -\left(\bar{\phi}_\epsilon(\boldsymbol{x}_t) - \textit{target}\right),$$

which is used to update the latent variable $\boldsymbol{z}_t$ (*via* $\boldsymbol{x}_t = \mathcal{D}(\boldsymbol{z}_t)$) through proximal Langevin dynamics.

		Generative Methods		
Ground	P(%)	*Cond*	*PDM*	*(Ours)*
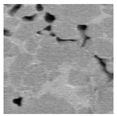	*30*	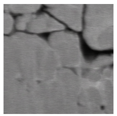	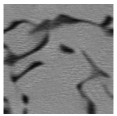	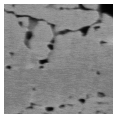
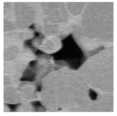	*50*	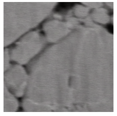	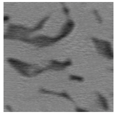	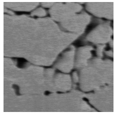
FID scores:		**10.8±0.9**	30.7±6.8	13.5±3.1
P error > 10%:		68.4%±12.4	**0%±0**	**0%±0**

Figure 1: Comparison of model performance in terms of FID score and constraint satisfaction (percentage of samples that does not satisfy the target porosity with a margin of 10%).

Voids diameter distribution

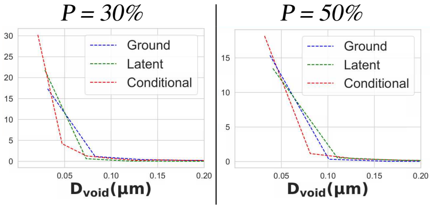

MSE w.r.t. Ground	
Cond: 1.58 **Ours: 0.47**	Cond: 0.31 **Ours: 0.12**

Figure 2: Distribution of void diameters in the training set (Ground) and in data generated by Conditional diffusion model and Latent Constrained Diffusion models.

6 Experiments

The performance of our method is evaluated in three domains, highlighting its applicability to diverse settings. Supplementary results and baselines are discussed in Appendices E and F.

Baselines. In each setting, performance is benchmarked against a series of baselines.

1. **Conditional Diffusion Model (Cond):** To assess the contribution of latent diffusion itself, we include a reference baseline consisting of an identical Stable Diffusion with text-conditioned constraints guidance [37].
2. **Projected Diffusion Models (PDM):** Following [15], this approach enforces feasibility by projecting onto the constraint set at each denoising step in the image space. PDM represents the current state-of-the-art for constrained generation in Sections 6.1 and 6.3.
3. **Bastek and Kochmann (2023):** For the task in Section 6.2, where PDM is inapplicable, we compare with this specialized method, which constitutes the state-of-the-art in that domain [38].

Collectively, these baselines capture the strongest existing constrained-generation methods, enabling a clear assessment of the improvements introduced by our latent constrained diffusion framework.

6.1 Microstructure Generation

Microstructure imaging data is critical in material science domains for discovering structure-property linkages. However, the availability of this data is limited on account of prohibitive costs to obtain high-resolution images of these microstructures. In this experiment, we task the model with generating samples subject to a constraint on the porosity levels of the output microstructures. Specifically, the goal is to generate new microstructures with specified, and often previously unobserved, porosity levels from a limited dataset of microstructure materials.

For this experiment we obtain the dataset used by [15, 39]. Notably, there are two significant obstacles to using this dataset: *data sparsity* and *absence of feasible samples*. To address the former limitation, we subsample the original microstructure images to generate the dataset using 64×64 images patches that have been upscaled to 1024×1024. To the latter point, while the dataset contains many samples that fall within lower porosity ranges, it is much more sparse at higher porosities. Hence, when constraining the porosity in these cases, often no feasible samples exist at a given porosity level.

Inner minimizer. To model the proximal operator for our proposed method, we use a projection operator in the image space and optimize with respect to this objective. Let $\boldsymbol{x}^{\boldsymbol{i},\boldsymbol{j}}$ be the pixel value for row i and column j, where $\boldsymbol{x}^{i,j} \in [-1, 1]$ for all values of i and j. The porosity is then,

$$\textit{porosity} = \sum_{i=1}^{n} \sum_{j=1}^{m} \mathbb{1}\left(\boldsymbol{x}^{i,j} < 0\right),$$

where $\mathbb{1}(\cdot)$ is the indicator function, which evaluates to 1 if the condition inside holds and 0 otherwise. We can then construct a projection using a top-k algorithm to return,

$$\mathcal{P}_{\mathbf{C}}(\boldsymbol{x}) = \operatorname*{argmin}_{\boldsymbol{y}^{i,j}} \sum_{i,j} \|\boldsymbol{y}^{i,j} - \boldsymbol{x}^{i,j}\| \qquad \text{s.t.} \quad \forall\, \boldsymbol{y}^{i,j} \in [-1,1], \quad \sum_{i=1}^{n}\sum_{j=1}^{m} \mathbb{1}\left(\boldsymbol{y}^{i,j} < 0\right) = K$$

where K is the number of pixels that should be "porous". Importantly, since the above program is convex, our model provides a certificate on the satisfaction of such constraints in the generated materials. We refer the interested reader to Appendix G for additional discussion.

Results. A sample of the results of our experiments is presented in Figure 1. Compared to the *Projected Diffusion Model (PDM)*, latent diffusion approaches show a significant improvement. Latent diffusion models enable higher-quality and higher-resolution images. The previous state-of-the-art PDM, which operates without latent diffusion, had an *FID more than twice as high as the models incorporating latent diffusion*. Alternatively, the *Conditional Diffusion Model*, utilizing text-to-image conditioning, reports the best average FID of 10.8 but performs poorly with regard to other evaluation metrics. Conditioning via text prompts proved unsuitable for enforcing the porosity constraints, and on average, *only 31.6% of the samples had a porosity error less than 10%,* indicating that this method lacks reliability in constraint satisfaction despite its ability to match the training distribution. Furthermore, as shown in Figure 2, the conditional model performs significantly worse than our method on producing realistic microstructures.

Model	MSE [↓]	*Fraction of physically invalid shapes* [↓]
Cond	7.1±4.5	55%
Bastek and Kochmann	6.4±4.6	20%
Latent (Ours)	**1.4±0.6**	**5**%

Figure 3: Compare MSE w.r.t. target stress-strain response and rejection rate of physically inconsistent shapes.

In contrast, our *Latent Constrained Model* exhibits the most optimal characteristics. The proposed method satisfies the porosity constraints *exactly*, achieves an excellent FID scores, and provides the *highest level of microstructure realism* as assessed by the heuristic-based analysis. This indicates that our approach effectively balances constraint satisfaction with high-quality image generation. *This is a significant advantage over existing baselines, as the method ensures both high-quality image generation and precise adherence to the physical constraints.*

6.2 Metamaterial Inverse Design

Now, we demonstrate the efficacy of our method for inverse-design of mechanical metamaterials with specific nonlinear stress-strain behaviors. Achieving desired mechanical responses necessitates precise control over factors such as buckling, contact interactions, and large-strain deformations, which are inherently nonlinear and sensitive to small parametric variations. Traditional design approaches often rely on trial-and-error methods, which are time-consuming and may not guarantee optimal solutions.

Specifically, our task is to generate mechanical metamaterials that closely match a target stress-strain response. From [38], we obtain a dataset of periodic stochastic cellular structures subjected to large-strain compression. This dataset includes full-field data capturing

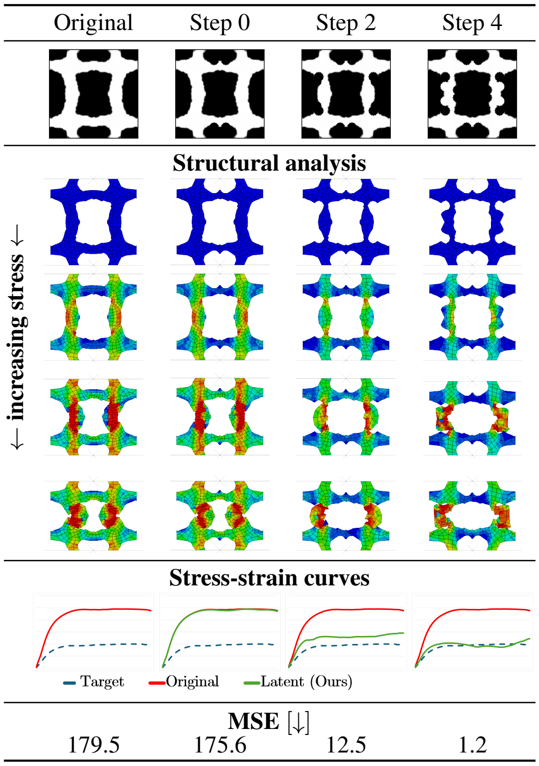

Figure 4: Successive steps of DPO. The sample is iteratively improved and the stress-strain curve aligns with the target. Structural analysis shows progressive deformation under controlled compression.

complex phenomena such as buckling and contact interactions. Because the problem is invariant with respect to length scale, the geometric variables can be treated as dimensionless. The stress is expressed in megapascals (MPa).

Inner minimizer. Exact constraint evaluation requires the use of *an external, non-differentiable simulator* ϕ. Hence, we employ DPO as described in Section 5 to facilitate the proximal mapping with respect to the signals provided from this module. To compute the ground truth results for the stress-strain response, we employ Abaqus [40], using this simulator both for our correction steps and for validation of the accuracy of the generations. For this implementation, we set the number of perturbed samples $M = 10$, finding this provides strong enough approximations of the gradients to converge to feasible solutions.

Results. We illustrate the DPO process for our *Latent Constrained Model* in Figure 4. Firstly, note that our method facilitates the reduction of error tolerance in our projection to arbitrarily low levels. By reducing the tolerance and performing additional DPO iterations, we can tighten the bound on the projection operator, thereby enhancing its accuracy. Moreover, the integration of the simulator enables the model to generalize beyond the confines of the existing dataset (see Figure 7).

Due to the complexity of the stress-strain response constraints in this problem, other constraint-aware methods (i.e. Projected Diffusion Models) are inapplicable, and, hence, our analysis focuses on the performance of *Conditional Diffusion Model* baselines. We compare to **(1)** an unconstrained stable diffusion model identical to the one used for our method and **(2)** state-of-the-art method proposed by Bastek and Kochmann [38], which operates in the ambient space. While our approach optimizes samples to arbitrary levels of precision, we observe that these baselines exhibit high error bounds relative to the target stress-strain curves that are unable to be further optimized. As shown in Figure 3, with five DPO steps our method provides a *4.6x improvement* over the state-of-the-art model by [38] and a *5.1x improvement* over the conditional stable diffusion model MSE between the predicted structure stress-strain response and target response. *These results demonstrate the efficacy of our approach for inverse-design problems and generating samples that adhere to the target properties.*

6.3 Copyright-Safe Generation

Next, we explore the applicability of the proposed method for satisfying surrogate constraints. An important challenge for safe deployment of generative models is mitigating the risk of generating outputs which closely resemble copyrighted material. For this setting, a pretrained proxy model is fine-tuned to determine whether the generation infringes upon existing copyrighted material. This model has been calibrated so that the output logits can be directly used to evaluate the likelihood that the samples resemble existing protected material. Hence, by minimizing this surrogate constraint function, we directly minimize the likelihood that the output image includes copyrighted material.

To implement this, we define a permissible threshold for the likelihood function captured by the classifier. A balanced dataset of 8,000 images is constructed to fine-tune the classifier and diffusion models. Here, we use cartoon mouse characters ‘Jerry,’ from *Tom and Jerry*, and copyright-protected character ‘Mickey Mouse’. When fine-tuning the diffusion model, we do not discriminate between these two characters, but the classifier is tuned to identify ‘Mickey Mouse’ as a copyrighted example.

Inner minimizer. Our correction step begins by performing Principal Component Analysis (PCA) on the 512 features input to the last layer and selecting the two principal components. This analysis yields two well-defined clusters corresponding to the class labels. Provided this, the inner minimizer differentiates with respect to a projection of the noisy sample onto the centroid of the target cluster, as illustrated in Figure 5 (top-right). Given the complexity of the constraints, we define a Lagrangian relaxation of the projection, terminating the iterative optimization based on proximity to the ‘Jerry’ cluster. Empirically, we found it was only necessary to trigger this proximal update if the classifier assigns a high probability to the sample being ‘Mickey Mouse’ at a given step.

Results. Figure 5 (bottom-right) reports the FID and constraint satisfaction, and Figure 5 (top-left) compares the evolution of the original sample and corrected sample. We implement a *Conditional Diffusion Model* baselines using and unconstrained stable diffusion model identical to the one used for our method. The conditional baseline generates the protected cartoon character (Mickey Mouse) *33% of the time*, despite conditioning it against these generations. The *Projected Diffusion Model* also struggles in this domain, particularly due to the image-space architecture’s inability to handle high dimensional data as effectively as the latent models; it failed to generate reasonable samples at

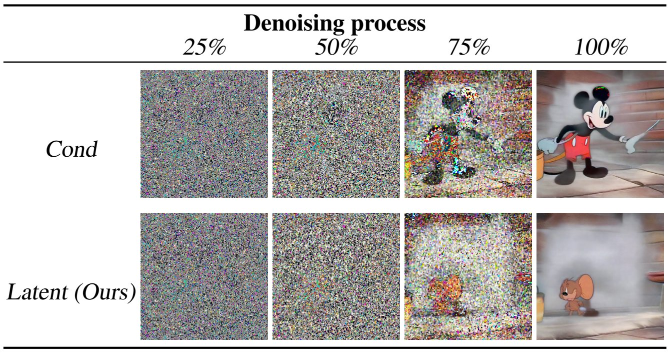

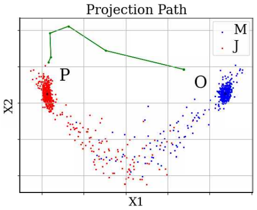

Model	Constraint [↑]	FID [↓]
Cond	67 %	**61.2**
PDM	71 %	75.3
Latent (Ours)	**90 %**	65.1

Figure 5: **Left:** Denoising process of Cond vs. Latent (Ours). Out method drives the denoising toward a copyright-safe image. **Top-right:** Showing projection from original (O) to projected (P) in the PCA-2 space. **Bottom-right:** Constraint satisfaction and FID scores.

a resolution of 1024×1024, unlike the latent models which maintained image quality at this scale. As a result, we were constrained to operate at a much lower resolution of 64×64 during sampling, subsequently relying on post-hoc upscaling techniques to reach the target resolution. This led to higher FID scores and only marginal improvement over the conditional model's constraint satisfaction. Conversely, our *Latent Constrained Model* only generates the protected cartoon character 10% of the time, aligning with the expected bounds of the classifier's predictive accuracy. Our method has proven to be highly effective because it preserves the generative capabilities of the model while imposing the defined constraints. The FID scores of the generated images remain largely unaltered by the gradient-based correction. *This demonstrates that our approach can selectively modify generated content to avoid copyrighted material without compromising overall image quality.*

7 Conclusion

This paper provides the first work integrating constrained optimization into the sampling process of stable diffusion models. This intersection enables the generation of outputs that both resemble the training data and adhere to task-specific constraints. By leveraging differentiable constraint evaluation functions within a constrained optimization framework, the proposed method ensures the feasibility of generated samples while maintaining high-quality synthesis. Experimental results in material science and safety-critical domains highlight the model's ability to meet strict property requirements and mitigate risks, such as copyright infringement. This approach paves the way for broader and more responsible applications of diffusion in domains where strict adherence to constraints is paramount.

Contributions

FF and JC conceived the idea and developed the initial methods. SZ and JC implemented the algorithms, contributed to discussions, and refined the research direction. SZ conducted the experiments and analysis, while JC contributed to theoretical development and additional experiments. FF provided overall guidance and coordination. JC, FF, and SZ co-wrote the paper. LO and DA funded SZ's visit to FF's lab.

Acknowledgments

The material is based upon work supported by National Science Foundations (NSF) awards 2533631, 2401285, 2334448, and 2334936, and Defense Advanced Research Projects Agency (DARPA) under Contract No. #HR0011252E005. The authors acknowledge Research Computing at the University of Virginia for providing computational resources that have contributed to the results reported within this paper. The views and conclusions of this work are those of the authors only.

References

[1] Jascha Sohl-Dickstein, Eric Weiss, Niru Maheswaranathan, and Surya Ganguli. Deep unsupervised learning using nonequilibrium thermodynamics. In *International conference on machine learning*, pages 2256–2265. PMLR, 2015.

[2] Jonathan Ho, Ajay Jain, and Pieter Abbeel. Denoising diffusion probabilistic models. *Advances in neural information processing systems*, 33:6840–6851, 2020.

[3] Tsun-Hsuan Wang, Juntian Zheng, Pingchuan Ma, Yilun Du, Byungchul Kim, Andrew Spielberg, Joshua Tenenbaum, Chuang Gan, and Daniela Rus. Diffusebot: Breeding soft robots with physics-augmented generative diffusion models. *arXiv preprint arXiv:2311.17053*, 2023.

[4] Ziyuan Zhong, Davis Rempe, Danfei Xu, Yuxiao Chen, Sushant Veer, Tong Che, Baishakhi Ray, and Marco Pavone. Guided conditional diffusion for controllable traffic simulation. In *2023 IEEE International Conference on Robotics and Automation (ICRA)*, pages 3560–3566. IEEE, 2023.

[5] Joao Carvalho, An T Le, Mark Baierl, Dorothea Koert, and Jan Peters. Motion planning diffusion: Learning and planning of robot motions with diffusion models. In *2023 IEEE/RSJ International Conference on Intelligent Robots and Systems (IROS)*, pages 1916–1923. IEEE, 2023.

[6] Michael Janner, Yilun Du, Joshua B Tenenbaum, and Sergey Levine. Planning with diffusion for flexible behavior synthesis. *arXiv preprint arXiv:2205.09991*, 2022.

[7] Namrata Anand and Tudor Achim. Protein structure and sequence generation with equivariant denoising diffusion probabilistic models. *arXiv preprint arXiv:2205.15019*, 2022.

[8] Emiel Hoogeboom, Vıctor Garcia Satorras, Clément Vignac, and Max Welling. Equivariant diffusion for molecule generation in 3d. In *International conference on machine learning*, pages 8867–8887. PMLR, 2022.

[9] Chentao Cao, Zhuo-Xu Cui, Yue Wang, Shaonan Liu, Taijin Chen, Hairong Zheng, Dong Liang, and Yanjie Zhu. High-frequency space diffusion model for accelerated mri. *IEEE Transactions on Medical Imaging*, 2024.

[10] Hyungjin Chung and Jong Chul Ye. Score-based diffusion models for accelerated mri. *Medical image analysis*, 80:102479, 2022.

[11] Robin Rombach, Andreas Blattmann, Dominik Lorenz, Patrick Esser, and Björn Ommer. High-resolution image synthesis with latent diffusion models, 2022. URL `https://arxiv.org/abs/2112.10752`.

[12] Thomas Frerix, Matthias Nießner, and Daniel Cremers. Homogeneous linear inequality constraints for neural network activations. In *Proceedings of the IEEE/CVF Conference on Computer Vision and Pattern Recognition Workshops*, pages 748–749, 2020.

[13] Nic Fishman, Leo Klarner, Valentin De Bortoli, Emile Mathieu, and Michael Hutchinson. Diffusion models for constrained domains. *arXiv preprint arXiv:2304.05364*, 2023.

[14] Nic Fishman, Leo Klarner, Emile Mathieu, Michael Hutchinson, and Valentin De Bortoli. Metropolis sampling for constrained diffusion models. *Advances in Neural Information Processing Systems*, 36, 2024.

[15] Jacob K Christopher, Stephen Baek, and Ferdinando Fioretto. Constrained synthesis with projected diffusion models, 2024.

[16] Guan-Horng Liu, Tianrong Chen, Evangelos Theodorou, and Molei Tao. Mirror diffusion models for constrained and watermarked generation. *Advances in Neural Information Processing Systems*, 36, 2024.

[17] Bowen Song, Soo Min Kwon, Zecheng Zhang, Xinyu Hu, Qing Qu, and Liyue Shen. Solving inverse problems with latent diffusion models via hard data consistency. *arXiv preprint arXiv:2307.08123*, 2023.

[18] Rayhan Zirvi, Bahareh Tolooshams, and Anima Anandkumar. Diffusion state-guided projected gradient for inverse problems. *arXiv preprint arXiv:2410.03463*, 2024.

[19] Litu Rout, Negin Raoof, Giannis Daras, Constantine Caramanis, Alex Dimakis, and Sanjay Shakkottai. Solving linear inverse problems provably via posterior sampling with latent diffusion models. *Advances in Neural Information Processing Systems*, 36:49960–49990, 2023.

[20] Jesse Engel, Matthew Hoffman, and Adam Roberts. Latent constraints: Learning to generate conditionally from unconditional generative models, 2017.

[21] Lei Shi and Andreas Bulling. Clad: Constrained latent action diffusion for vision-language procedure planning. *arXiv preprint arXiv:2503.06637*, 2025.

[22] Yang Song and Stefano Ermon. Generative modeling by estimating gradients of the data distribution. *Advances in neural information processing systems*, 32, 2019.

[23] Yang Song, Jascha Sohl-Dickstein, Diederik P Kingma, Abhishek Kumar, Stefano Ermon, and Ben Poole. Score-based generative modeling through stochastic differential equations. *arXiv preprint arXiv:2011.13456*, 2020.

[24] Robin Rombach, Andreas Blattmann, Dominik Lorenz, Patrick Esser, and Björn Ommer. High-resolution image synthesis with latent diffusion models. In *Proceedings of the IEEE/CVF Conference on Computer Vision and Pattern Recognition*, pages 10684–10695, 2022.

[25] Dustin Podell, Zion English, Kyle Lacey, Andreas Blattmann, Tim Dockhorn, Jonas Müller, Joe Penna, and Robin Rombach. Sdxl: Improving latent diffusion models for high-resolution image synthesis. *arXiv preprint arXiv:2307.01952*, 2023.

[26] Max Welling and Yee W Teh. Bayesian learning via stochastic gradient langevin dynamics. In *Proceedings of the 28th international conference on machine learning (ICML-11)*, pages 681–688. Citeseer, 2011.

[27] Pan Xu, Jinghui Chen, Difan Zou, and Quanquan Gu. Global convergence of langevin dynamics based algorithms for nonconvex optimization. *Advances in Neural Information Processing Systems*, 31, 2018.

[28] Neal Parikh and Stephen Boyd. Proximal algorithms. *Foundations and Trends in Optimization*, 1(3):127–239, 2014.

[29] Patrick L Combettes and Jean-Christophe Pesquet. Proximal splitting methods in signal processing. *Fixed-point algorithms for inverse problems in science and engineering*, pages 185–212, 2011.

[30] Nicolas Brosse, Alain Durmus, Éric Moulines, and Marcelo Pereyra. Sampling from a log-concave distribution with compact support with proximal langevin monte carlo. In *Conference on learning theory*, pages 319–342. PMLR, 2017.

[31] R Tyrrell Rockafellar and Roger J-B Wets. *Variational analysis*, volume 317. Springer Science & Business Media, 2009.

[32] Magnus R Hestenes. Multiplier and gradient methods. *Journal of optimization theory and applications*, 4(5):303–320, 1969.

[33] Ferdinando Fioretto, Pascal Van Hentenryck, Terrence W. K. Mak, Cuong Tran, Federico Baldo, and Michele Lombardi. Lagrangian duality for constrained deep learning. In *European Conference on Machine Learning*, volume 12461 of *Lecture Notes in Computer Science*, pages 118–135. Springer, 2020. doi: 10.1007/978-3-030-67670-4_8. URL `https://doi.org/10.1007/978-3-030-67670-4_8`.

[34] Jiayi Guo, Xingqian Xu, Yifan Pu, Zanlin Ni, Chaofei Wang, Manushree Vasu, Shiji Song, Gao Huang, and Humphrey Shi. Smooth diffusion: Crafting smooth latent spaces in diffusion models. In *Proceedings of the IEEE/CVF Conference on Computer Vision and Pattern Recognition*, pages 7548–7558, 2024.

[35] Quentin Berthet, Mathieu Blondel, Olivier Teboul, Marco Cuturi, Jean-Philippe Vert, and Francis Bach. Learning with differentiable pertubed optimizers. *Advances in neural information processing systems*, 33:9508–9519, 2020.

[36] Jayanta Mandi, James Kotary, Senne Berden, Maxime Mulamba, Victor Bucarey, Tias Guns, and Ferdinando Fioretto. Decision-focused learning: Foundations, state of the art, benchmark and future opportunities. *Journal of Artificial Intelligence Research*, 80:1623–1701, 2024.

[37] Michail Dontas, Yutong He, Naoki Murata, Yuki Mitsufuji, J Zico Kolter, and Ruslan Salakhutdinov. Blind inverse problem solving made easy by text-to-image latent diffusion. *arXiv preprint arXiv:2412.00557*, 2024.

[38] Jan-Hendrik Bastek and Dennis M Kochmann. Inverse design of nonlinear mechanical metamaterials via video denoising diffusion models. *Nature Machine Intelligence*, 5(12):1466–1475, 2023.

[39] Sehyun Chun, Sidhartha Roy, Yen Thi Nguyen, Joseph B Choi, HS Udaykumar, and Stephen S Baek. Deep learning for synthetic microstructure generation in a materials-by-design framework for heterogeneous energetic materials. *Scientific reports*, 10(1):13307, 2020.

[40] L Börgesson. Abaqus. In *Developments in geotechnical engineering*, volume 79, pages 565–570. Elsevier, 1996.

[41] Jonathan Ho and Tim Salimans. Classifier-free diffusion guidance. *arXiv preprint arXiv:2207.12598*, 2022.

[42] Ye Yuan, Jiaming Song, Umar Iqbal, Arash Vahdat, and Jan Kautz. Physdiff: Physics-guided human motion diffusion model. In *Proceedings of the IEEE/CVF International Conference on Computer Vision*, pages 16010–16021, 2023.

[43] Prafulla Dhariwal and Alexander Nichol. Diffusion models beat gans on image synthesis. *Advances in neural information processing systems*, 34:8780–8794, 2021.

[44] Hyungjin Chung, Jeongsol Kim, Michael T Mccann, Marc L Klasky, and Jong Chul Ye. Diffusion posterior sampling for general noisy inverse problems. *arXiv preprint arXiv:2209.14687*, 2022.

[45] Joao Carvalho, A Le, Piotr Kicki, Dorothea Koert, and Jan Peters. Motion planning diffusion: Learning and adapting robot motion planning with diffusion models. *arXiv preprint arXiv:2412.19948*, 2024.

[46] Jiwen Yu, Yinhuai Wang, Chen Zhao, Bernard Ghanem, and Jian Zhang. Freedom: Training-free energy-guided conditional diffusion model. In *Proceedings of the IEEE/CVF International Conference on Computer Vision*, pages 23174–23184, 2023.

[47] Sicheng Mo, Fangzhou Mu, Kuan Heng Lin, Yanli Liu, Bochen Guan, Yin Li, and Bolei Zhou. Freecontrol: Training-free spatial control of any text-to-image diffusion model with any condition. In *Proceedings of the IEEE/CVF Conference on Computer Vision and Pattern Recognition*, pages 7465–7475, 2024.

[48] Yutong He, Naoki Murata, Chieh-Hsin Lai, Yuhta Takida, Toshimitsu Uesaka, Dongjun Kim, Wei-Hsiang Liao, Yuki Mitsufuji, J Zico Kolter, Ruslan Salakhutdinov, et al. Manifold preserving guided diffusion. *arXiv preprint arXiv:2311.16424*, 2023.

[49] Arpit Bansal, Hong-Min Chu, Avi Schwarzschild, Soumyadip Sengupta, Micah Goldblum, Jonas Geiping, and Tom Goldstein. Universal guidance for diffusion models. In *Proceedings of the IEEE/CVF Conference on Computer Vision and Pattern Recognition*, pages 843–852, 2023.

[50] Haotian Ye, Haowei Lin, Jiaqi Han, Minkai Xu, Sheng Liu, Yitao Liang, Jianzhu Ma, James Zou, and Stefano Ermon. Tfg: Unified training-free guidance for diffusion models. *arXiv preprint arXiv:2409.15761*, 2024.

[51] William Huang, Yifeng Jiang, Tom Van Wouwe, and C Karen Liu. Constrained diffusion with trust sampling. *arXiv preprint arXiv:2411.10932*, 2024.

[52] Thomas Power, Rana Soltani-Zarrin, Soshi Iba, and Dmitry Berenson. Sampling constrained trajectories using composable diffusion models. In *IROS 2023 Workshop on Differentiable Probabilistic Robotics: Emerging Perspectives on Robot Learning*, 2023.

[53] Giorgio Giannone, Akash Srivastava, Ole Winther, and Faez Ahmed. Aligning optimization trajectories with diffusion models for constrained design generation. *arXiv preprint arXiv:2305.18470*, 2023.

[54] François Mazé and Faez Ahmed. Diffusion models beat gans on topology optimization. In *Proceedings of the AAAI Conference on Artificial Intelligence (AAAI), Washington, DC*, 2023.

[55] Andrea Coletta, Sriram Gopalakrishnan, Daniel Borrajo, and Svitlana Vyetrenko. On the constrained time-series generation problem. *Advances in Neural Information Processing Systems*, 36:61048–61059, 2023.

[56] Kartik Sharma, Srijan Kumar, and Rakshit Trivedi. Diffuse, sample, project: plug-and-play controllable graph generation. In *Forty-first International Conference on Machine Learning*, 2024.

[57] Stephen P Boyd and Lieven Vandenberghe. *Convex optimization*. Cambridge university press, 2004.

NeurIPS Paper Checklist

1. **Claims**

   Question: Do the main claims made in the abstract and introduction accurately reflect the paper's contributions and scope?

   Answer: [Yes]

   Justification: The claims made in the abstract are theoretically and empirically supported by the content of the paper. We include proofs for all theoretical claims and three distinct, real-world settings to evaluate the proposed methodology.

   Guidelines:

   - The answer NA means that the abstract and introduction do not include the claims made in the paper.
   - The abstract and/or introduction should clearly state the claims made, including the contributions made in the paper and important assumptions and limitations. A No or NA answer to this question will not be perceived well by the reviewers.
   - The claims made should match theoretical and experimental results, and reflect how much the results can be expected to generalize to other settings.
   - It is fine to include aspirational goals as motivation as long as it is clear that these goals are not attained by the paper.

2. **Limitations**

   Question: Does the paper discuss the limitations of the work performed by the authors?

   Answer: [Yes]

   Justification: Limitations are discussed in a standalone section (Appendix A).

   Guidelines:

   - The answer NA means that the paper has no limitation while the answer No means that the paper has limitations, but those are not discussed in the paper.
   - The authors are encouraged to create a separate "Limitations" section in their paper.
   - The paper should point out any strong assumptions and how robust the results are to violations of these assumptions (e.g., independence assumptions, noiseless settings, model well-specification, asymptotic approximations only holding locally). The authors should reflect on how these assumptions might be violated in practice and what the implications would be.
   - The authors should reflect on the scope of the claims made, e.g., if the approach was only tested on a few datasets or with a few runs. In general, empirical results often depend on implicit assumptions, which should be articulated.
   - The authors should reflect on the factors that influence the performance of the approach. For example, a facial recognition algorithm may perform poorly when image resolution is low or images are taken in low lighting. Or a speech-to-text system might not be used reliably to provide closed captions for online lectures because it fails to handle technical jargon.
   - The authors should discuss the computational efficiency of the proposed algorithms and how they scale with dataset size.
   - If applicable, the authors should discuss possible limitations of their approach to address problems of privacy and fairness.
   - While the authors might fear that complete honesty about limitations might be used by reviewers as grounds for rejection, a worse outcome might be that reviewers discover limitations that aren't acknowledged in the paper. The authors should use their best judgment and recognize that individual actions in favor of transparency play an important role in developing norms that preserve the integrity of the community. Reviewers will be specifically instructed to not penalize honesty concerning limitations.

3. **Theory assumptions and proofs**

   Question: For each theoretical result, does the paper provide the full set of assumptions and a complete (and correct) proof?

Answer: [Yes]

Justification: Proofs for all theoretical results are included in Appendix H. These proofs are complete and correct to the best of our knowledge.

Guidelines:

- The answer NA means that the paper does not include theoretical results.
- All the theorems, formulas, and proofs in the paper should be numbered and cross-referenced.
- All assumptions should be clearly stated or referenced in the statement of any theorems.
- The proofs can either appear in the main paper or the supplemental material, but if they appear in the supplemental material, the authors are encouraged to provide a short proof sketch to provide intuition.
- Inversely, any informal proof provided in the core of the paper should be complemented by formal proofs provided in appendix or supplemental material.
- Theorems and Lemmas that the proof relies upon should be properly referenced.

4. **Experimental result reproducibility**

   Question: Does the paper fully disclose all the information needed to reproduce the main experimental results of the paper to the extent that it affects the main claims and/or conclusions of the paper (regardless of whether the code and data are provided or not)?

   Answer: [Yes]

   Justification: Our experimental section and Appendix E provide all necessary details to reporduce our work (e.g., datasets, implementation details, etc.).

   Guidelines:

   - The answer NA means that the paper does not include experiments.
   - If the paper includes experiments, a No answer to this question will not be perceived well by the reviewers: Making the paper reproducible is important, regardless of whether the code and data are provided or not.
   - If the contribution is a dataset and/or model, the authors should describe the steps taken to make their results reproducible or verifiable.
   - Depending on the contribution, reproducibility can be accomplished in various ways. For example, if the contribution is a novel architecture, describing the architecture fully might suffice, or if the contribution is a specific model and empirical evaluation, it may be necessary to either make it possible for others to replicate the model with the same dataset, or provide access to the model. In general. releasing code and data is often one good way to accomplish this, but reproducibility can also be provided via detailed instructions for how to replicate the results, access to a hosted model (e.g., in the case of a large language model), releasing of a model checkpoint, or other means that are appropriate to the research performed.
   - While NeurIPS does not require releasing code, the conference does require all submissions to provide some reasonable avenue for reproducibility, which may depend on the nature of the contribution. For example
     (a) If the contribution is primarily a new algorithm, the paper should make it clear how to reproduce that algorithm.
     (b) If the contribution is primarily a new model architecture, the paper should describe the architecture clearly and fully.
     (c) If the contribution is a new model (e.g., a large language model), then there should either be a way to access this model for reproducing the results or a way to reproduce the model (e.g., with an open-source dataset or instructions for how to construct the dataset).
     (d) We recognize that reproducibility may be tricky in some cases, in which case authors are welcome to describe the particular way they provide for reproducibility. In the case of closed-source models, it may be that access to the model is limited in some way (e.g., to registered users), but it should be possible for other researchers to have some path to reproducing or verifying the results.

5. **Open access to data and code**

Question: Does the paper provide open access to the data and code, with sufficient instructions to faithfully reproduce the main experimental results, as described in supplemental material?

Answer: [Yes]

Justification: We provide code with our submission and intend to release a public repository following the reviewing process.

Guidelines:

- The answer NA means that paper does not include experiments requiring code.
- Please see the NeurIPS code and data submission guidelines (`https://nips.cc/public/guides/CodeSubmissionPolicy`) for more details.
- While we encourage the release of code and data, we understand that this might not be possible, so "No" is an acceptable answer. Papers cannot be rejected simply for not including code, unless this is central to the contribution (e.g., for a new open-source benchmark).
- The instructions should contain the exact command and environment needed to run to reproduce the results. See the NeurIPS code and data submission guidelines (`https://nips.cc/public/guides/CodeSubmissionPolicy`) for more details.
- The authors should provide instructions on data access and preparation, including how to access the raw data, preprocessed data, intermediate data, and generated data, etc.
- The authors should provide scripts to reproduce all experimental results for the new proposed method and baselines. If only a subset of experiments are reproducible, they should state which ones are omitted from the script and why.
- At submission time, to preserve anonymity, the authors should release anonymized versions (if applicable).
- Providing as much information as possible in supplemental material (appended to the paper) is recommended, but including URLs to data and code is permitted.

6. **Experimental setting/details**

   Question: Does the paper specify all the training and test details (e.g., data splits, hyperparameters, how they were chosen, type of optimizer, etc.) necessary to understand the results?

   Answer: [Yes]

   Justification: We include these details when applicable.

   Guidelines:

   - The answer NA means that the paper does not include experiments.
   - The experimental setting should be presented in the core of the paper to a level of detail that is necessary to appreciate the results and make sense of them.
   - The full details can be provided either with the code, in appendix, or as supplemental material.

7. **Experiment statistical significance**

   Question: Does the paper report error bars suitably and correctly defined or other appropriate information about the statistical significance of the experiments?

   Answer: [Yes]

   Justification: We have included error bars in our experimental results.

   Guidelines:

   - The answer NA means that the paper does not include experiments.
   - The authors should answer "Yes" if the results are accompanied by error bars, confidence intervals, or statistical significance tests, at least for the experiments that support the main claims of the paper.
   - The factors of variability that the error bars are capturing should be clearly stated (for example, train/test split, initialization, random drawing of some parameter, or overall run with given experimental conditions).

- The method for calculating the error bars should be explained (closed form formula, call to a library function, bootstrap, etc.)
- The assumptions made should be given (e.g., Normally distributed errors).
- It should be clear whether the error bar is the standard deviation or the standard error of the mean.
- It is OK to report 1-sigma error bars, but one should state it. The authors should preferably report a 2-sigma error bar than state that they have a 96% CI, if the hypothesis of Normality of errors is not verified.
- For asymmetric distributions, the authors should be careful not to show in tables or figures symmetric error bars that would yield results that are out of range (e.g. negative error rates).
- If error bars are reported in tables or plots, The authors should explain in the text how they were calculated and reference the corresponding figures or tables in the text.

8. **Experiments compute resources**

   Question: For each experiment, does the paper provide sufficient information on the computer resources (type of compute workers, memory, time of execution) needed to reproduce the experiments?

   Answer: [Yes]

   Justification: We describe the used resources in Appendix F.

   Guidelines:

   - The answer NA means that the paper does not include experiments.
   - The paper should indicate the type of compute workers CPU or GPU, internal cluster, or cloud provider, including relevant memory and storage.
   - The paper should provide the amount of compute required for each of the individual experimental runs as well as estimate the total compute.
   - The paper should disclose whether the full research project required more compute than the experiments reported in the paper (e.g., preliminary or failed experiments that didn't make it into the paper).

9. **Code of ethics**

   Question: Does the research conducted in the paper conform, in every respect, with the NeurIPS Code of Ethics `https://neurips.cc/public/EthicsGuidelines`?

   Answer: [Yes]

   Justification: All ethical standards have been observed in conducting this research.

   Guidelines:

   - The answer NA means that the authors have not reviewed the NeurIPS Code of Ethics.
   - If the authors answer No, they should explain the special circumstances that require a deviation from the Code of Ethics.
   - The authors should make sure to preserve anonymity (e.g., if there is a special consideration due to laws or regulations in their jurisdiction).

10. **Broader impacts**

    Question: Does the paper discuss both potential positive societal impacts and negative societal impacts of the work performed?

    Answer: [NA]

    Justification: The societal impacts of this work are common to other advancements in machine learning. As these are general and well-known by those in the field, we do not expressly highlighted them.

    Guidelines:

    - The answer NA means that there is no societal impact of the work performed.
    - If the authors answer NA or No, they should explain why their work has no societal impact or why the paper does not address societal impact.

- Examples of negative societal impacts include potential malicious or unintended uses (e.g., disinformation, generating fake profiles, surveillance), fairness considerations (e.g., deployment of technologies that could make decisions that unfairly impact specific groups), privacy considerations, and security considerations.
- The conference expects that many papers will be foundational research and not tied to particular applications, let alone deployments. However, if there is a direct path to any negative applications, the authors should point it out. For example, it is legitimate to point out that an improvement in the quality of generative models could be used to generate deepfakes for disinformation. On the other hand, it is not needed to point out that a generic algorithm for optimizing neural networks could enable people to train models that generate Deepfakes faster.
- The authors should consider possible harms that could arise when the technology is being used as intended and functioning correctly, harms that could arise when the technology is being used as intended but gives incorrect results, and harms following from (intentional or unintentional) misuse of the technology.
- If there are negative societal impacts, the authors could also discuss possible mitigation strategies (e.g., gated release of models, providing defenses in addition to attacks, mechanisms for monitoring misuse, mechanisms to monitor how a system learns from feedback over time, improving the efficiency and accessibility of ML).

11. **Safeguards**

    Question: Does the paper describe safeguards that have been put in place for responsible release of data or models that have a high risk for misuse (e.g., pretrained language models, image generators, or scraped datasets)?

    Answer: [NA]

    Justification: This paper does not deal with data or models that pose high risks.

    Guidelines:

    - The answer NA means that the paper poses no such risks.
    - Released models that have a high risk for misuse or dual-use should be released with necessary safeguards to allow for controlled use of the model, for example by requiring that users adhere to usage guidelines or restrictions to access the model or implementing safety filters.
    - Datasets that have been scraped from the Internet could pose safety risks. The authors should describe how they avoided releasing unsafe images.
    - We recognize that providing effective safeguards is challenging, and many papers do not require this, but we encourage authors to take this into account and make a best faith effort.

12. **Licenses for existing assets**

    Question: Are the creators or original owners of assets (e.g., code, data, models), used in the paper, properly credited and are the license and terms of use explicitly mentioned and properly respected?

    Answer: [Yes]

    Justification: All assets include are used in the capacity allowed by their respective licenses, and the original owners have been properly cited.

    Guidelines:

    - The answer NA means that the paper does not use existing assets.
    - The authors should cite the original paper that produced the code package or dataset.
    - The authors should state which version of the asset is used and, if possible, include a URL.
    - The name of the license (e.g., CC-BY 4.0) should be included for each asset.
    - For scraped data from a particular source (e.g., website), the copyright and terms of service of that source should be provided.

- If assets are released, the license, copyright information, and terms of use in the package should be provided. For popular datasets, `paperswithcode.com/datasets` has curated licenses for some datasets. Their licensing guide can help determine the license of a dataset.
- For existing datasets that are re-packaged, both the original license and the license of the derived asset (if it has changed) should be provided.
- If this information is not available online, the authors are encouraged to reach out to the asset's creators.

13. **New assets**

    Question: Are new assets introduced in the paper well documented and is the documentation provided alongside the assets?

    Answer: [NA]

    Justification: No new assets are provided by this paper.

    Guidelines:

    - The answer NA means that the paper does not release new assets.
    - Researchers should communicate the details of the dataset/code/model as part of their submissions via structured templates. This includes details about training, license, limitations, etc.
    - The paper should discuss whether and how consent was obtained from people whose asset is used.
    - At submission time, remember to anonymize your assets (if applicable). You can either create an anonymized URL or include an anonymized zip file.

14. **Crowdsourcing and research with human subjects**

    Question: For crowdsourcing experiments and research with human subjects, does the paper include the full text of instructions given to participants and screenshots, if applicable, as well as details about compensation (if any)?

    Answer: [NA]

    Justification: No human subjects were involved in this research.

    Guidelines:

    - The answer NA means that the paper does not involve crowdsourcing nor research with human subjects.
    - Including this information in the supplemental material is fine, but if the main contribution of the paper involves human subjects, then as much detail as possible should be included in the main paper.
    - According to the NeurIPS Code of Ethics, workers involved in data collection, curation, or other labor should be paid at least the minimum wage in the country of the data collector.

15. **Institutional review board (IRB) approvals or equivalent for research with human subjects**

    Question: Does the paper describe potential risks incurred by study participants, whether such risks were disclosed to the subjects, and whether Institutional Review Board (IRB) approvals (or an equivalent approval/review based on the requirements of your country or institution) were obtained?

    Answer: [NA]

    Justification: The paper does not involve crowdsourcing nor research with human subjects.

    Guidelines:

    - The answer NA means that the paper does not involve crowdsourcing nor research with human subjects.
    - Depending on the country in which research is conducted, IRB approval (or equivalent) may be required for any human subjects research. If you obtained IRB approval, you should clearly state this in the paper.

- We recognize that the procedures for this may vary significantly between institutions and locations, and we expect authors to adhere to the NeurIPS Code of Ethics and the guidelines for their institution.
- For initial submissions, do not include any information that would break anonymity (if applicable), such as the institution conducting the review.

16. **Declaration of LLM usage**

    Question: Does the paper describe the usage of LLMs if it is an important, original, or non-standard component of the core methods in this research? Note that if the LLM is used only for writing, editing, or formatting purposes and does not impact the core methodology, scientific rigorousness, or originality of the research, declaration is not required.

    Answer: [NA]

    Justification: LLMs were not involved in the core method development.

    Guidelines:

    - The answer NA means that the core method development in this research does not involve LLMs as any important, original, or non-standard components.
    - Please refer to our LLM policy (`https://neurips.cc/Conferences/2025/LLM`) for what should or should not be described.

A Limitation

Classifier-based constraints. Section 6.3 motivates the use of classifier-based constraints for stable diffusion models. While we illustrate one potential use case of this approach, we hold that this can generalize to arbitrary properties that can be captured using a classifier. We defer more rigorous comparison to classifier guidance [2] and classifier-free guidance [41] for future work.

Stable video generation. While there many exciting applications for using this approach for scientific and safety-critical domains when generating data in the image space, many more applications will be enabled by extending this work to video diffusion models. While we compare to video diffusion baselines in Section 6.2, our training-free correction algorithm is only applied to stable image diffusion models. The introduction of temporal constraints over video frames holds significant potential that we plan to investigate in subsequent studies.

Integration of external simulators. This paper motivates future study of embedding non-differentiable simulators within generative process. Yuan et al. [42] previously proposed the inclusion of physics-based simulators to augment diffusion generations, but in their case, differentiability was not considered as their simulation used a reinforcement-learning environment to directly return a modified version of the noisy sample $\boldsymbol{x}_t$. More often, external simulators are used to provide a measure of constraint satisfaction rather than to transform a sample. The techniques explored in this paper provide a vastly more general framework for incorporating these black-box simulators as a differentiable components of the sampling process and, hence, opens the door for the integration of increasingly complex constraints. Further use cases will be explored in consecutive works.

B Related Work

Conditional diffusion guidance. Conditional diffusion models have emerged as a powerful tool to guide generative models toward specific tasks. Classifier-based [43] and classifier-free [41] conditioning methods have been employed to frame higher-level constraints for inverse design problems [3, 10, 38, 44] and physically grounding generations [5, 42, 45]. Rombach et al. extended conditional guidance to stable diffusion models via class-conditioning, allowing similar guidance schemes to be applied for latent generation. However, while conditioning based approaches can effectively capture class-level specifications, they are largely ineffective when lower-level properties need to be satisfied (as demonstrated in Section 6.1).

Training-free diffusion guidance. Similar to classifier-based conditioning, training-free guidance approaches leverage an external classifier to guide generations to satisfy specific constraints. Juxtaposed to classifier-based conditioning, and the method proposed in this paper, training-free guidance leverages *off-the-shelf* classifiers which have been trained exclusively on clean data. Several approaches have been proposed which incorporate slight variations of training-free guidance to improve constraint adherence [46–49]. Ye et al. compose a unified view of these methods, detailing search strategies to optimize the implementation of this paradigm. Huang et al. improve constraint adherence by introducing a "trust schedule" that increases the strength of the guidance as the reverse process progresses but remain unable to exactly satisfy the constraint set, even within the statistical bounds of the employed classifier. Importantly, training-free guidance approaches suffer from two significant shortcomings. First, this paradigm exhibits worse performance than classifier-based guidance as the off-the-shelf classifiers provide inaccurate gradients at higher noise levels. Second, like classifier-based guidance, these guidance schemes are ineffective in satisfying lower-level constraints

Post-processing optimization. When strict constraints are required, diffusion outputs are frequently used as initial guesses for a subsequent constrained optimization procedure. This approach has been shown to be particularly advantageous in non-convex scenarios where the initial starting point strongly influences convergence to a feasible solution [52]. Other methods incorporate optimization objectives directly into the diffusion training process, essentially framing the post-processing optimization steps as an extension of the generative model [53, 54]. However, these methods rely on a succinctly formulated objective and therefore often remain effective only for niche problems—such as constrained trajectory optimization—limiting their applicability to a wider set of generative tasks. Furthermore, post-processing steps are agnostic to the original data distribution, and, hence, the constraint correction steps often results in divergence from this distribution altogether. This has been empirically demonstrated in previous studies on constrained diffusion model generation [15].

Hard constraints for generative models. Frerix et al. [12] proposed an approach to impose hard constraints on autoencoder outputs by scaling the generated data so that feasibility is enforced, but this solution is limited to simple linear constraints. Liu et al. [16] introduced "mirror mappings" to handle constraints, though their method applies solely to familiar convex constraint sets. Given the complex constraints examined in this paper, neither of these strategies was suitable for our experiments. Alternatively, Fishman et al. [13, 14] extended the classes of constraints that can be handled, but their approach is demonstrated only for trivial predictive tasks with MLPs where constraints can be represented as convex polytopes. This confines their method to constraints approximated by simple geometric shapes, such as L2-balls, simplices, or polytopes. Coletta et al. [55] provide a generalization of constrained diffusion approaches for time-series problems, and, while these settings are not explored in our work, we take inspiration from their framing of diffusion sampling as a constrained optimization framework. Most similar to our work are Sharma et al. [56] and Christopher et al. [15], concurrent studies which propose projected Langevin dynamics sampling processes for constrained generation tasks. Sharma et al. [56] develop this approach for constrained graph generation, making this work not directly applicable to the tasks explored in this work. Christopher et al. generalize this sampling process for arbitrary constraint sets, but, like the other methods for hard constraint imposition discussed, their work is not extended to stable diffusion models.

Stable diffusion for constrained settings. Although inverse design has been extensively studied in diffusion models operating directly in image space, fewer studies have investigated the potential of stable diffusion models for inverse design, as these models have primarily been applied in commercial rather than scientific contexts. Song et al. [17] propose *ReSample*, which repurposed latent diffusion models as inverse-problem solvers by alternating a hard data-consistency projection and stochastic resampling steps returning the sample to the learned manifold. While applicable to image reconstruction with a fixed measurement operator, this approach cannot be adapted to handle open-ended constraint sets as explored in this work as it assumes knowledge of this operator for the data-consistency projection. More recently, Zirvi et al. [18] follow-up on this line of research, demonstrating improvement over [17] and [19], a method proposed concurrently to *ReSample*, but all three methods are limited in the requirement of a forward measurement operator which does not appear in our explored settings. This dependency narrows the scope of these inverse design methods, and this rigid definition of inverse design problems similarly restricts the applicability similarly presented methodology for diffusion operating in the image space.

Notably, a handful of other works explore constrained settings more generally without requiring dependency on the measurement operator. Engel et al. [20] proposes learning the constraints in the latent space via a neural operator, applying this methodology to auto-encoder architectures. Although effective for soft constraint conditioning, our attempts to adapt such approaches to latent diffusion were unsuccessful and such approaches can be viewed as a weaker alternative to classifier-based conditional guidance. Rather, conditioning approaches such as proposed by [24] have proven much stronger alternatives, leading to our selection of constraint-conditioned stable diffusion as a baseline throughout the explored settings. Finally, concurrent to our study, Shi and Bulling [21] proposes *CLAD* for imposing *learned* constraints on latent diffusion model generations, but, importantly, their study has very different objectives than our work. As opposed to our work, which enables imposition of hard constraints at inference time, *CLAD* learns latent vectors to statistically optimize feasibility for visual planning tasks. Importantly, this approach outputs symbolic action tokens as opposed to high-resolution pixel images, a distinctly disconnected modality from those explored in this paper.

C Comparison to Classifier Guidance

At first glance, this approach might appear similar to classifier-guided diffusion [43], as both rely on an external predictive model to direct the generation process. However, the two methods fundamentally differ in how the methods apply the model's gradient. Classifier-guided diffusion encourages similarity to feasible training samples, offering implicit guidance. In contrast, our approach provides *statistical guarantees as to constraint satisfaction within the confidence levels of the classifier,* providing a more direct and targeted mechanism for integrating constraints into the generative process.

Classifier-based guidance. Applies Bayesian principles to direct generation toward a target class y, based on the decomposition:

$$\nabla_{\boldsymbol{x}_t} \log p(\boldsymbol{x}_t \mid y) = \nabla_{\boldsymbol{x}_t} \log p(\boldsymbol{x}_t) + \nabla_{\boldsymbol{x}_t} \log p(y \mid \boldsymbol{x}_t) \tag{9}$$

This conditional generation incorporates a classifier $p(y \mid \boldsymbol{x}_t)$ into the sampling process. During generation, the model updates the noisy sample $\boldsymbol{x}_t$ by combining the standard denoising step with the classifier's gradient:

$$x_{t+1} = x_t + \epsilon \nabla_{x_t} \log p(x_t) + \sqrt{2\epsilon} + w \nabla_{x_t} \log p(y \mid x_t) \tag{10}$$

Here, the classifier's gradient $w\nabla_{x_t} \log p(y \mid \boldsymbol{x}_t)$ guides the denoising toward samples likely belonging to class y, with w controlling the guidance strength.

Training-free guidance. Extends the principles of classifier-based guidance by leveraging pretrained, "off-the-shelf" classifiers to steer the generation process without requiring additional training. As with classifier-based guidance, the conditional generation incorporates a classifier $p(y \mid \boldsymbol{x}_t)$ into the sampling process. However, rather than training a custom classifier tailored to the diffusion model, this approach directly uses existing models to compute the guidance term. By decoupling the classifier from the diffusion model training, training-free guidance achieves flexibility and reusability, making it a practical choice for tasks where suitable pretrained classifiers are available.

Surrogate constraint corrections. Introduce a structured method to enforce class-specific constraints by adjusting samples at specific diffusion steps. In this approach, a surrogate model modifies the sample $\mathbf{z}_t$ to $\hat{\mathbf{z}}_t$ to meet the target constraints. These corrections can be introduced either at the beginning of the diffusion process, setting a strong initial alignment to the target class and then allowing the model to evolve naturally, or at designated points within the denoising sequence to enforce the constraints more explicitly at each selected step. In contrast, while classifier-based guidance and training-free guidance continuously integrate classifier gradients to steer generation toward the target class, surrogate constraint corrections offer discrete, targeted adjustments throughout the reverse diffusion process. This makes surrogate constraints particularly effective when strict adherence to certain class-specific conditions is necessary at particular stages of the generation process.

D Augmented Lagrangian Method

In experimental settings 6.2 and 6.3, a closed-form projection operator cannot be derived in the image space, and it becomes necessary to solve this subproblem through gradient-based relaxations. In these settings, we adopt the *Augmented Lagrangian Method* to facilitate this relaxation [57]. This method operated by restructuring a constrained optimization problem, in our case

$$\arg\min_{y \in \mathbf{C}} \|\boldsymbol{y} - \mathcal{D}(\mathbf{z}_t)\|$$

as a minimization objective which captures feasibility constraints through penalty terms. Expressly, the use of Lagrangian multipliers $\lambda = (\lambda_1, \ldots, \lambda_n)$ and quadratic penalty terms $\mu = (\mu_1, \ldots, \mu_n)$ form the *dual variables* used to solve the relaxation. Hence, the objective becomes:

$$\arg\min_{\boldsymbol{y}} \|\boldsymbol{y} - \mathcal{D}(\mathbf{z}_t)\| + \lambda\, \mathbf{g}(\boldsymbol{y}) + \tfrac{\mu}{2}\, \mathbf{g}(\boldsymbol{y})^2.$$

This problem provides a lower-bound approximation to the original projection. Its Lagrangian dual solves:

$$\arg\max_{\lambda,\mu} \Big(\arg\min_{\boldsymbol{y}} \|\boldsymbol{y} - \mathcal{D}(\mathbf{z}_t)\| + \lambda\, \mathbf{g}(\boldsymbol{y}) + \tfrac{\mu}{2}\, \mathbf{g}(\boldsymbol{y})^2\Big).$$

Following the dual updates described by [33], we perform the following updates:

$$\boldsymbol{y} \leftarrow \boldsymbol{y} - \gamma \nabla_{\boldsymbol{y}} \mathcal{L}_{\text{ALM}}\big(\boldsymbol{y}, \lambda, \mu\big), \tag{11a}$$

$$\lambda \leftarrow \lambda + \mu\, \tilde{\phi}(\boldsymbol{y}), \tag{11b}$$

$$\mu \leftarrow \min(\alpha\mu, \mu_{\max}), \tag{11c}$$

where γ is the gradient step size, $\alpha > 1$ is a scalar which increases μ over iterations, and $\mu_{\max}$ is an upper bound on μ. This drives $\boldsymbol{y}$ to satisfy $g(\boldsymbol{y}) \approx 0$ while staying close to $\mathcal{D}(\mathbf{z}_t)$.

Algorithm 2: Augmented Lagrangian

```
Input: $\boldsymbol{x}_t, \lambda, \mu, \gamma, \alpha, \delta$
$\boldsymbol{y} \leftarrow \mathcal{D}(\mathbf{z}_t)$
while $\tilde{\phi}(\boldsymbol{y}) < \delta$ do
    for $j \leftarrow 1$ to max_inner_iter do
        $\mathcal{L}_{\text{ALM}} \leftarrow$
            $\|\boldsymbol{y} - \mathcal{D}(\mathbf{z}_t)\| + \lambda\, \mathbf{g}(\boldsymbol{y}) + \frac{\mu}{2}\, \mathbf{g}(\boldsymbol{y})^2$
        $\boldsymbol{y} \leftarrow \boldsymbol{y} - \gamma\, \nabla_{\boldsymbol{y}} \mathcal{L}_{\text{ALM}}$
    $\lambda \leftarrow \lambda + \mu\, \tilde{\phi}(\boldsymbol{y})$;
    $\mu \leftarrow \min\big(\alpha\mu,\ \mu_{\max}\big)$
return $\boldsymbol{y}$
```

E Extended Results

In this section, we include additional results and figures from our experimental evaluation.

E.1 Microstructure Generation

Additional baselines. To supplement the evaluation presented in paper, we also implemented the following baselines:

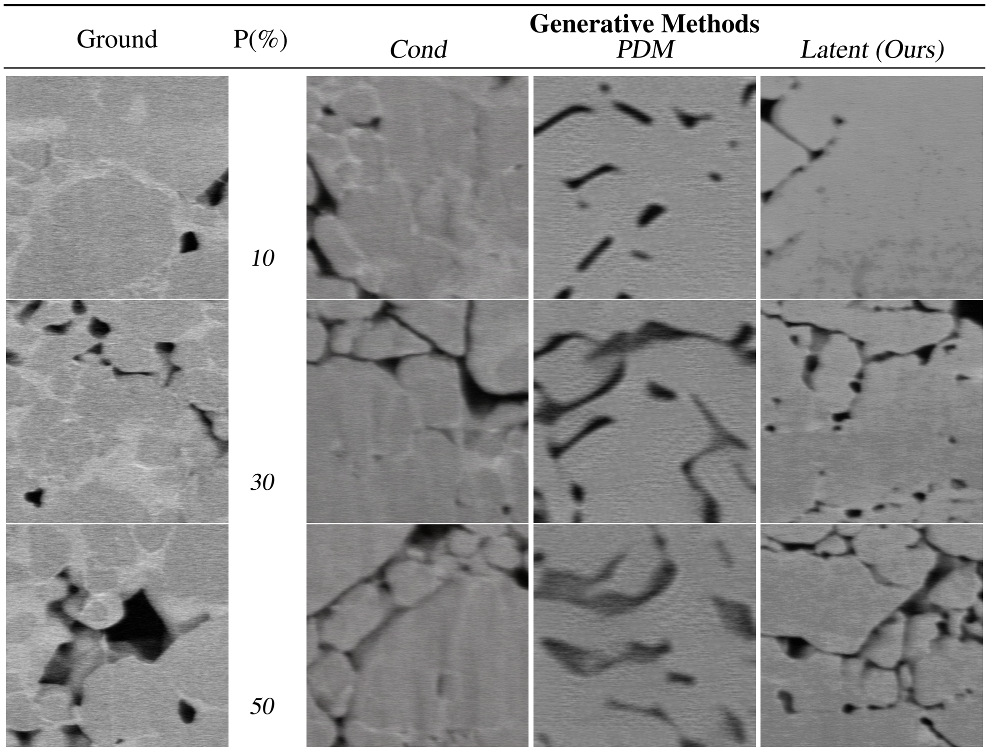

	Cond	PDM	Latent (Ours)
FID scores:	10.8±0.9	30.7±6.8	13.5±3.1
P error > 10%:	68.4%±12.4	0%±0	0%±0

Figure 6: Extended version of Figure 1

1. **Image Space Correction:** We implement a naive approach which converts the latent representation to the image space, projects the image, and then passes the feasible image through the encoder layer to return to the latent space.
2. **Learned Latent Corrector:** Adapting the implementation by [20] for diffusion models, we train a network to restore feasibility prior to the decoding step.

The *Image Space Correction* method, which involves re-encoding the image into the latent space after correcting it during various denoising steps, and the *Learned Latent Corrector* method, where a network is trained to project a latent vector toward a new state ensuring constraint satisfaction, both failed to produce viable samples. **Both baselines deviated significantly from the training set distribution,** resulting in high FID scores and generated images that lacked quality, failing to capture essential features of the dataset. Due to the inability of these methods to produce viable samples, we do not include them in Figure 1.

E.2 Metamaterial Inverse Design

Figure 7 illustrates the performance of different models in interpolation (i.e., when the target curve falls within the stress range covered by the training set) and in extrapolation (i.e., when the target is outside this range). In addition to the proposed model, a Conditional Stable Diffusion model and a Conditional Video Diffusion model [38] are shown. The proposed model allows for arbitrarily small tolerance settings and outperforms the baselines in both tests.

Practically, one can select an error tolerance and compute budget for tailored for the specific application. Each iteration of the DPO necessitates approximately 30 seconds of computational time. Given our prescribed error tolerance, convergence is achieved within five iterations, culminating in a total computational duration of approximately 2.5 minutes per optimization run. Additionally, note that ϕ has not been optimized for runtime, operating exclusively on CPU cores.

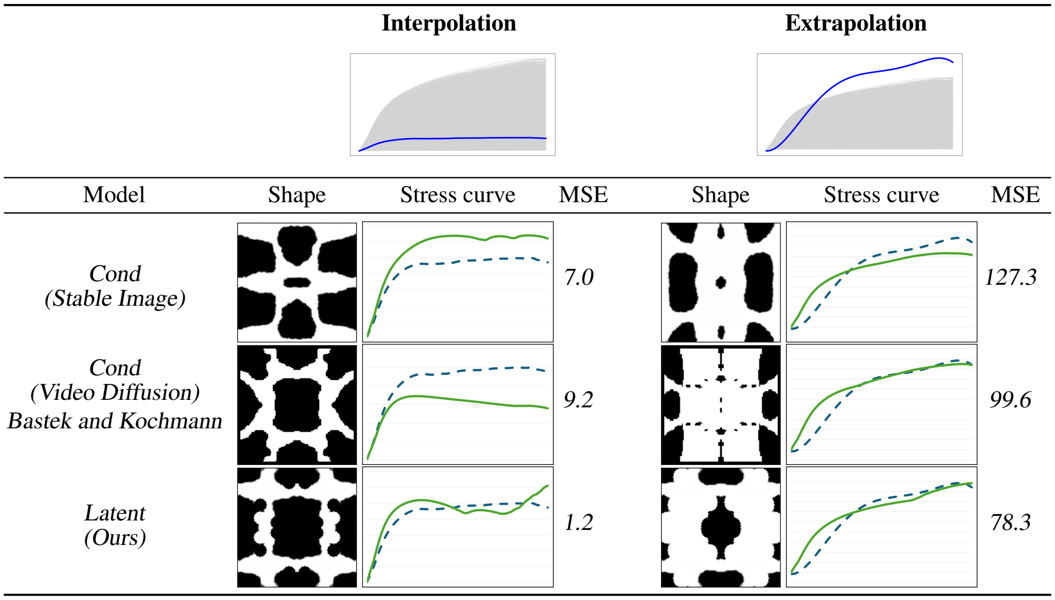

Figure 7: Performance of different models in interpolation and in extrapolation.

E.3 Copyright-Safe Generation

As opposed to other approaches, the projection schedule is tuned differently for this setting. Particularly, it is only necessary to project during the initial stages of the generation. After this correction, the denoising process is allowed to evolve naturally without further intervention. This method ensures that the generated images are guided away from resembling copyrighted material while still allowing the model to produce high-quality outputs. By selectively modifying the generated content during the initial stages of denoising, we can effectively prevent the model from producing images that infringe on copyrights without significantly affecting the overall image quality.

Surrogate implementation. We begin by fine-tuning a classifier capable of predicting membership to one of two classes: ‘Mickey Mouse’ or ‘Jerry’. The architecture of the classifier consists of a ResNet50 backbone, which is followed by two fully connected layers. These layers serve to progressively reduce the dimensionality of the feature map, first from 2048 to 512 and then from 512 to a single scalar feature, which represents the output of the classifier. A Sigmoid activation function is then applied to this final feature to estimate the probability that the input sample belongs to either the ‘Mickey Mouse’ or ‘Jerry’ class. This process ensures that the model outputs a value between 0 and 1, indicating the likelihood of each class membership. The classifier was evaluated on a held-out test set and demonstrated a strong performance, achieving an accuracy greater than 87%, which showcases its effectiveness in distinguishing between the two classes.

F Runtime

Note that the simulator employed in Section 6.2 has been specifically optimized for CPU execution; consequently, runtimes observed for these experiments are inherently longer compared to GPU-optimized procedures (refer to Table F). Importantly, optimizing computational runtime was not the primary focus of this study. Rather, the emphasis was placed on scientific discovery, prioritizing the fidelity and accuracy of the generated content. In the scientific domains explored, achieving exact adherence to physical constraints and established principles is crucial, as deviations would render the models unreliable and impractical for use.

A significant bottleneck frequently encountered in these experimental domains is the iterative cycle from experimental design to validation, which typically necessitates multiple trial-and-error iterations. Consequently, the capability to generate realistic synthetic materials exhibiting precisely controlled morphological or structural characteristics, as demonstrated at the fidelity levels reported herein, holds substantial potential for accelerating scientific workflows—from initial experimentation to full-scale production.

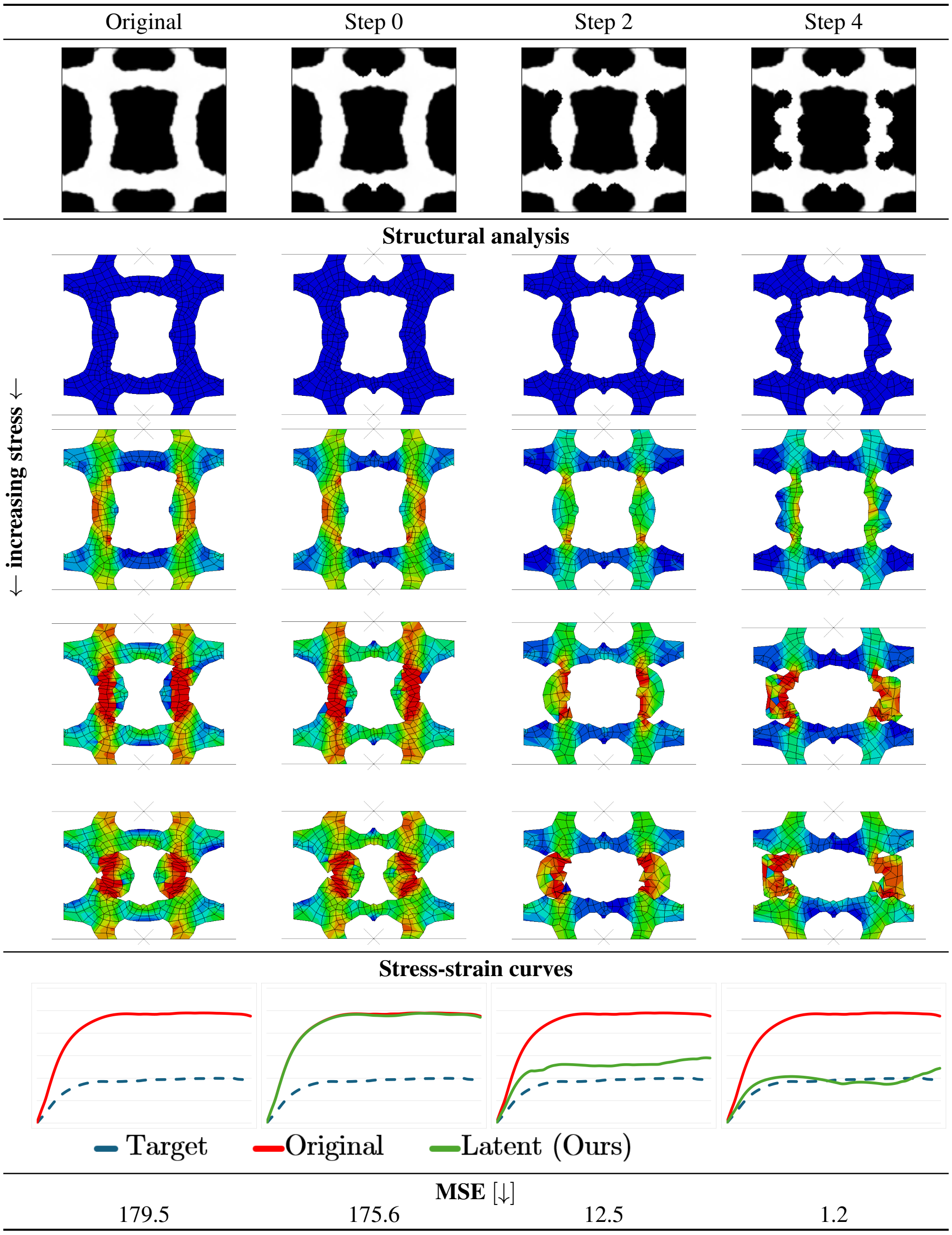

Figure 8: Enlarged version of Figure 4. Successive steps of DPO are shown. At each stage, M perturbed shapes are generated, each undergoing structural analysis with ϕ, which provides the corresponding stress-strain. The perturbation that produces the curve closest to the target is then selected, and a new perturbation-structural analysis-selection cycle begins, continuing until convergence is achieved. The convergence tolerance can be tightened as desired, provided it is compatible with the available computational cost.

Experiment	Sampling Type	Time	Hardware
Microstructure	Conditional Sampling	10 s	Nvidia A100-SXM4-80GB
Microstructure	Constrained Sampling	50 s	Nvidia A100-SXM4-80GB
Metamaterials	Conditional Sampling	5 s	Nvidia A100-SXM4-80GB
Metamaterials	Single Simulation	30 s	Intel Core i7-8550U CPU
Copyright	Conditional Sampling	10 s	Nvidia A100-SXM4-80GB
Copyright	Constrained Sampling	65 s	Nvidia A100-SXM4-80GB

Table 1: Experiment runtimes by sampling type and hardware.

G Feasibility Guarantees

First, note that when a projection (or approximation thereof) can be constructed in the image space, strict guarantees can be provided on the feasibility of the *final outputs* of the stable diffusion model. A final projection can be applied after decoding $\mathbf{z}_0$, and, as this operator is applied directly in the image space, constraint satisfaction is ensured if the projection is onto a convex set. As detailed in [57](§8.1), a projection of any vector $\boldsymbol{x} \in \mathbb{R}^n$ onto a non-empty closed convex set $\mathbf{C}$ exists and is unique.

Theorem G.1. ***Convex Constraint Guarantees:*** *The proposed method provides feasibility guarantees for convex constraint.*

As we can derive a closed-form projection for convex sets in the ambient space after decoding our sample (e.g., in Section 6.1 where our proximal operator used is a projection), the proposed method thus provides guarantees for convex constraints.

H Supplementary Proofs

H.1 Proof of Theorem 4.1 (Part 1): Non-Asymptotic Feasibility in the Image Space

Proof. We begin by proving this bound holds for projected diffusion methods operating in the image space:

$$\operatorname{dist}\big(\boldsymbol{x}'_t, \boldsymbol{C}\big)^2 \;\leq\; (1 - 2\beta\gamma_{t+1})\, \operatorname{dist}\big(\boldsymbol{x}'_{t+1}, \boldsymbol{C}\big)^2 + \gamma_{t+1}^2 G^2, \tag{12}$$

For clarity and simplicity of this proof, we omit superscripts in subsequent iterations, using only subscripts to denote both inner and outer iterations of the Langevin sampler. For instance, the sequence $\boldsymbol{x}_t^0, \ldots, \boldsymbol{x}_t^M, \boldsymbol{x}_{t-1}^0$ is now represented as $\boldsymbol{x}_t, \ldots, \boldsymbol{x}_{t-M}, \boldsymbol{x}_{t-(M+1)}$. Consequently, as annealing occurs at the outer loop level (every M iterations), the step size γ_t is no longer strictly decreasing with each iteration t, and instead satisfies $\gamma_t \geq \gamma_{t-1}$.

Consider that at each iteration of the denoising process, projected diffusion methods can be split into two steps:

1. **Gradient Step:** $\boldsymbol{x}'_t = \boldsymbol{x}_t + \gamma_t \underbrace{\nabla_{\boldsymbol{x}_t} \log q(\boldsymbol{x}_t)}_{s_t}$
2. **Projection Step:** $\boldsymbol{x}_{t-1} = \mathcal{P}_{\mathbf{C}}(\boldsymbol{x}'_t)$

These steps are sequentially applied in the reverse process to sample from a constrained subdistribution.

$$\boldsymbol{x}_t \to \overbrace{\boldsymbol{x}_t + \gamma_t s_t}^{\boldsymbol{x}'_t} \to \mathcal{P}_{\mathbf{C}}(\boldsymbol{x}'_t) = \boldsymbol{x}_{t-1} \to \overbrace{\boldsymbol{x}_{t-1} + \gamma_{t-1} s_{t-1}}^{\boldsymbol{x}'_{t-1}} \to \mathcal{P}_{\mathbf{C}}(\boldsymbol{x}'_{t-1}) = \boldsymbol{x}_{t-2} \ldots$$

By construction, $\boldsymbol{x}_{t-1} = \mathcal{P}_{\mathbf{C}}(\boldsymbol{x}'_t) \in \mathbf{C}$. Next, let us define the projection distance to $\mathbf{C}$ as:

$$f(\boldsymbol{x}) = \operatorname{dist}(\boldsymbol{x}, \mathbf{C})^2 = \|\boldsymbol{x} - \mathcal{P}_{\mathbf{C}}(\boldsymbol{x})\|^2$$

Since $\mathbf{C}$ is β-prox regular, by definition the following hold:

- f is differentiable outside $\mathbf{C}$ (in a neighborhood)
- $\nabla f(\boldsymbol{x}) = 2(\boldsymbol{x} - \mathcal{P}_{\mathbf{C}}(\boldsymbol{x}))$
- ∇f is L-Lipshitz with $L = \frac{2}{\beta}$

The "descent lemma" for L-smooth functions applies:

Lemma H.1. *$\forall \boldsymbol{x}, \boldsymbol{y}$ in the neighborhood of $\mathbf{C}$:*

$$f(\boldsymbol{y}) \leq f(\boldsymbol{x}) + \langle \nabla f(\boldsymbol{x}), \boldsymbol{y} - \boldsymbol{x} \rangle + \frac{L}{2}\|\boldsymbol{y} - \boldsymbol{x}\|^2 = \boxed{f(\boldsymbol{x}) + 2\langle \boldsymbol{x} - \mathcal{P}_{\mathbf{C}}(\boldsymbol{x}), \boldsymbol{y} - \boldsymbol{x} \rangle + \frac{1}{\beta}\|\boldsymbol{y} - \boldsymbol{x}\|^2}$$

Applying this lemma, let us use $\boldsymbol{x} = \boldsymbol{x}'_{t-1}$ and $\boldsymbol{y} = \boldsymbol{x}'_t$. Noting that $\mathcal{P}_{\mathbf{C}}(\boldsymbol{x}'_t) = \boldsymbol{x}_{t-1}$, we get:

$$\operatorname{dist}(\boldsymbol{x}'_t, \mathbf{C})^2 \leq \underbrace{\operatorname{dist}(\boldsymbol{x}'_{t-1}, \mathbf{C})^2}_{\text{Term A}} + \underbrace{2\,\langle \boldsymbol{x}'_{t-1} - \boldsymbol{x}_{t-2}, \boldsymbol{x}'_t - \boldsymbol{x}'_{t-1} \rangle}_{\text{Term B}} + \underbrace{\frac{1}{\beta}\|\boldsymbol{x}'_t - \boldsymbol{x}'_{t-1}\|^2}_{\text{Term C}} \tag{$\star$}$$

Decomposing Term B. First, consider that since the step size is decreasing $\gamma_t \geq \gamma_{t-1}$:

$$\begin{aligned} \boldsymbol{x}'_{t-1} - \boldsymbol{x}_{t-2} &\leq (\boldsymbol{x}_{t-1} - \boldsymbol{x}_{t-2}) + \gamma_{t-1} s_{t-1} \\ &\leq (\boldsymbol{x}_{t-1} - \boldsymbol{x}_{t-2}) + \gamma_t s_{t-1} \end{aligned}$$

By the same rationale,

$$\boldsymbol{x}'_t - \boldsymbol{x}'_{t-1} \leq (\boldsymbol{x}_t - \boldsymbol{x}_{t-1}) + \gamma_t(s_t - s_{t-1}). \tag{Definition B.1}$$

Proof of non-expansiveness of the projection operator. Next, we prove the non-expansiveness of the projection operator:

$$\|\boldsymbol{x}_t - \boldsymbol{x}_{t-1}\| \leq 2\,\gamma_{t+1} G^2 \tag{$\mathcal{L}^+$}$$

Given $\boldsymbol{x}_t = \mathcal{P}_{\mathbf{C}}(\boldsymbol{x}'_{t+1})$ and $\boldsymbol{x}_{t-1} = \mathcal{P}_{\mathbf{C}}(\boldsymbol{x}'_t)$,

$$\|\boldsymbol{x}_t - \boldsymbol{x}_{t-1}\| = \|\mathcal{P}_{\mathbf{C}}(\boldsymbol{x}'_{t+1}) - \mathcal{P}_{\mathbf{C}}(\boldsymbol{x}'_t)\| \leq \|\boldsymbol{x}_{t+1} - \boldsymbol{x}_t\|$$

since projections onto closed prox-regular sets are L-Lipshitz.

Now:

$$\begin{aligned} \boldsymbol{x}'_{t+1} &= \boldsymbol{x}_{t+1} + \gamma_{t+1} s_{t+1}; \\ \boldsymbol{x}'_t \quad &= \boldsymbol{x}_t + \gamma_t s_t; \\ \boldsymbol{x}'_{t+1} - \boldsymbol{x}'_t &= (\boldsymbol{x}_{t+1} - \boldsymbol{x}_t) + (\gamma_{t+1} s_{t+1} - \gamma_t s_t). \end{aligned} \tag{Definition B.2}$$

Making the projection residual,

$$\boldsymbol{x}_{t+1} - \boldsymbol{x}_t = \boldsymbol{x}_{t+1} - \mathcal{P}_{\mathbf{C}}(\boldsymbol{x}'_{t+1})$$

orthogonal to the target space at $\boldsymbol{x}_t$ (and any vector of the form $s_{t+1} - s_t$). Thus, since $\|s_t\| \leq G \;\; \forall t$:

$$\|\boldsymbol{x}'_{t+1} - \boldsymbol{x}'_t\|^2 = \|\gamma_{t+1} s_{t+1}\|^2 + \|\gamma_t s_t\| \leq (\gamma_{t+1}^2 + \gamma_t^2) G^2$$

Taking the square root:

$$\|\boldsymbol{x}'_{t+1} - \boldsymbol{x}'_t\| \leq \sqrt{\gamma_{t+1}^2 + \gamma_t^2}\, G$$

Since $\gamma_{t+1} \geq \gamma_t$:

$$\begin{aligned} \|\boldsymbol{x}'_{t+1} - \boldsymbol{x}'_t\| &\leq \sqrt{2}\gamma_{t+1} G \\ &< 2\gamma_{t+1} G \end{aligned}$$

Finally, by applying Definition (B.1), $\|\boldsymbol{x}_{t+1} - \boldsymbol{x}_t\| \leq \|\boldsymbol{x}'_{t+1} - \boldsymbol{x}'_t\|$, and thus:

$$\boxed{\|\boldsymbol{x}_{t+1} - \boldsymbol{x}_t\| \leq 2\gamma_{t+1} G}$$

□

Now, prox-regularity gives:

$$\begin{aligned} \langle \boldsymbol{x}'_{t-1} - \boldsymbol{x}_{t-2}, \boldsymbol{x}'_t - \boldsymbol{x}'_{t-1} \rangle &\leq \beta \|\boldsymbol{x}_t - \boldsymbol{x}_{t-1}\|^2 \\ &\leq 4\beta\gamma_{t+1}^2 G^2 \end{aligned} \tag{Bound B.1}$$

where the Bound B.1 is derived by applying ($\mathcal{L}^+$).

Since $\mathbf{C}$ in β-prox regular, for any point u near $\mathbf{C}$ and $v \in \mathbf{C}$:

$$\langle u - \mathcal{P}_{\mathbf{C}}(u), v - \mathcal{P}_{\mathbf{C}}(u)\rangle \leq \beta \|v - \mathcal{P}_{\mathbf{C}}(u)\|^2$$

Above, we substitute:

$$\begin{aligned} u &= \boldsymbol{x}_t' = \boldsymbol{x}_t + \gamma_t s_t \\ v &= \boldsymbol{x}_t \\ \mathcal{P}_{\mathbf{C}}(u) &= \boldsymbol{x}_{t-1} \end{aligned}$$

Now, expanding the inner product:

$$\begin{aligned} \langle \boldsymbol{x}_{t-1}' - \boldsymbol{x}_{t-2}, \boldsymbol{x}_t' - \boldsymbol{x}_{t-1}'\rangle &= \langle \boldsymbol{x}_{t-1}' - \boldsymbol{x}_{t-2}, (\boldsymbol{x}_t + \gamma_t s_t) - (\boldsymbol{x}_{t-1} + \gamma_{t-1} s_{t-1})\rangle \\ &\leq \langle \boldsymbol{x}_{t-1}' - \boldsymbol{x}_{t-2}, (\boldsymbol{x}_t - \boldsymbol{x}_{t-1}) + \gamma_t(s_t - s_{t-1})\rangle \\ &\leq \langle \boldsymbol{x}_{t-1}' - \boldsymbol{x}_{t-2}, (\boldsymbol{x}_t - \boldsymbol{x}_{t-1})\rangle + \langle \boldsymbol{x}_{t-1}' - \boldsymbol{x}_{t-2}, \gamma_t(s_t - s_{t-1})\rangle \end{aligned}$$

and since $\|s_t\| \leq G \quad \forall t$: $\langle s_{t+1}, s_t\rangle \leq \|s_{t+1}\|\|s_t\| \leq G^2$ so $\langle s_{t-1}, s_t\rangle - \|s_{t+1}\|^2 \leq G^2$, and:

$$\langle \boldsymbol{x}_{t-1}' - \boldsymbol{x}_{t-2}, \gamma_t(s_t - s_{t-1})\rangle \leq \gamma_t^2 G^2 \tag{Bound B.2}$$

By applying Definition (B.2):

$$\begin{aligned} \langle \boldsymbol{x}_{t-1}' - \boldsymbol{x}_{t-2}, \boldsymbol{x}_t' - \boldsymbol{x}_{t-1}'\rangle &= \langle \boldsymbol{x}_{t-1}' - \boldsymbol{x}_{t-2}, (\boldsymbol{x}_t - \boldsymbol{x}_t) + (\gamma_t s_t - \gamma_{t-1} s_{t-1})\rangle \\ &\leq \langle \boldsymbol{x}_{t-1}' - \boldsymbol{x}_{t-2}, (\boldsymbol{x}_t - \boldsymbol{x}_{t-1})\rangle \end{aligned}$$

Therefore, by applying Bound (B.1) to the previous inequality and Bound (B.2) directly, Term B is upper bounded by:

$$\boxed{2\,\langle \boldsymbol{x}_{t-1}' - \boldsymbol{x}_{t-2}, \boldsymbol{x}_t' - \boldsymbol{x}_{t-1}'\rangle \leq 8\beta\gamma_{t+1}^2 G^2 + 2\gamma_t^2 G^2} \tag{Bound B.3}$$

Decomposing Term C. Next, we derive a bound on Term C in Eq. ($\star$). As already shown,

$$\|\boldsymbol{x}_t' - \boldsymbol{x}_{t-1}'\| \leq 4\gamma_t G,$$

given:

$$\begin{aligned} \boldsymbol{x}_t' - \boldsymbol{x}_{t-1}' &\leq \underbrace{(\boldsymbol{x}_t - \boldsymbol{x}_{t-1})}_{\leq 2\gamma_{t+1} G} + \underbrace{\gamma_t(s_t - s_{t-1})}_{\leq 2G} \\ &\leq 4\gamma_{t+1} G \end{aligned}$$

Thus,

$$\boxed{\frac{1}{\beta}\|\boldsymbol{x}_t' - \boldsymbol{x}_{t-1}'\|^2 \leq \frac{16}{\beta}\gamma_{t+1}^2 G^2} \tag{Bound C.1}$$

Combining bounds (B.3) and (C.1) into ($\star$), and recalling that $\gamma_{t+1} \geq \gamma_t$:

$$\text{dist}(\boldsymbol{x}_t', \mathbf{C})^2 \leq \underbrace{\text{dist}(\boldsymbol{x}_{t-1}', \mathbf{C})^2}_{d} + \underbrace{(8\beta + 2 + \frac{16}{\beta})}_{K}\gamma_{t+1}^2 G^2$$

Now, we rewrite Term A, which for ease of notation we will refer to as d:

$$d^2 = (1 - 2\beta\gamma_{t+1})d^2 + 2\beta\gamma_{t+1} d^2$$

Thus:

$$\begin{aligned} \text{dist}(\boldsymbol{x}_t', \mathbf{C})^2 &\leq d^2 - 2\beta\gamma_{t+1} d^2 + 2\beta\gamma_{t+1} d^2 + K\gamma_{t+1}^2 G^2 \\ &= (1 - 2\beta\gamma_{t+1})d^2 + \left[2\beta\gamma_{t+1} d^2 + K\gamma_{t+1}^2 G^2\right] \end{aligned}$$

Next, through Young's inequality, we simplify this expression further.

Theorem H.2. **(Young's Inequality)** *$\forall u, v \geq 0, \epsilon > 0$:*

$$uv \leq \frac{u^2}{2\epsilon} + \frac{\epsilon v^2}{2}$$

If we choose $u = \sqrt{2\beta\gamma_{t+1}}d$, $v = \sqrt{K}\gamma_{t+1}G$, and $\epsilon = \frac{2\beta d^2}{k\gamma_{t+1}G^2}$, then

$$\begin{aligned} uv &= \sqrt{2\beta\gamma_{t+1}}d \times \sqrt{K}\gamma_{t+1}G \\ &= \sqrt{2K}\gamma_{t+1}^{\frac{3}{4}}Gd \end{aligned}$$

Applying Young's Inequality:

$$\begin{aligned} uv &\leq \frac{u^2}{2\epsilon} + \frac{\epsilon v^2}{2} \\ &= \frac{2\beta\gamma_{t+1}d^2}{2(\frac{2\beta d^2}{K\gamma_{t+1}G^2})} + \frac{\epsilon v^2}{2} \\ &= \frac{K\gamma_{t+1}^2G^2}{2} + \frac{\epsilon v^2}{2} \\ &= \frac{K\gamma_{t+1}^2G^2}{2} + \left(\frac{1}{2} \times \frac{2\beta d^2}{K\gamma_{t+1}G^2} \times K\gamma_{t+1}^2G^2\right) \\ &= \frac{K\gamma_{t+1}^2G^2}{2} + \beta\gamma_{t+1}d^2 \end{aligned}$$

Thus,

$$\sqrt{2K}\gamma_{t+1}^{\frac{3}{4}}Gd \leq \frac{K\gamma_{t+1}^2G^2}{2} + \beta\gamma_{t+1}d^2$$

Finally, taken altogether:

$$\begin{aligned} 2\beta\gamma_{t+1}d^2 + K\gamma_{t+1}^2G^2 &\leq \beta\gamma_{t+1}d^2 + \left(\frac{K\gamma_{t+1}^2G^2}{2} + \beta\gamma_{t+1}d^2\right) \\ &= 2\beta\gamma_{t+1}d^2 + \frac{K}{2}\gamma_{t+1}^2G^2 \end{aligned}$$

Since $\gamma_{t+1} \leq \frac{\beta}{2G^2}$, then

$$\frac{K}{2}\gamma_{t+1}^2G^2 \leq \frac{1}{2}\left(8\beta + 2 + \frac{16}{\beta}\right)\frac{\beta^2}{4G^2} = \mathcal{O}(\beta^3)$$

which is bounded by $\gamma_{t+1}^2G^2$ for all $\beta \geq 0$.

Thus,

$$2\beta\gamma_{t+1}d^2 + K\gamma_{t+1}^2G^2 \leq 2\beta\gamma_{t+1}d^2 + \gamma_{t+1}^2G^2.$$

Finally, by substitution:

$$\boxed{\text{dist}(\boldsymbol{x}'_t, \mathbf{C})^2 \leq (1 - 2\beta\gamma_{t+1})\text{dist}(\boldsymbol{x}'_{t-1}, \mathbf{C})^2 + \underbrace{\gamma_{t+1}^2G^2}_{\mathcal{O}(\beta^3)}}$$

□

H.2 Proof of Theorem 4.1 (Part 2): Non-Asymptotic Feasibility in the Latent Space

Proof. The previous proof can be naturally extended to latent space models under smoothness assumptions:

Assumption H.3.

(1) **(Decoder regularity)** $\mathcal{D} : \mathbb{R}^{d_z} \to \mathbb{R}^{d_x}$ is ℓ-Lipschitz and $\|\nabla\mathcal{D}(\mathbf{z})\|_{\text{op}} \leq \ell$ for all $\mathbf{z}$.

(2) **(Constraint regularity)** $g : \mathbb{R}^{d_x} \to \mathbb{R}^m$ is L-smooth and $\nabla g(\mathbf{x})$ has full row rank on $\mathbf{C} = \{\mathbf{x} : g(\mathbf{x}) = \mathbf{0}\}$, hence $\mathbf{C}$ is prox-regular.

Let $\mathbf{x}'_t = \mathcal{D}(\mathbf{z}'_t)$ be the decoded pre-projection iterate. Prox-regularity implies

$$\left\|\mathbf{x}_{t+1} - \mathcal{P}_{\mathbf{C}}(\mathbf{x}'_t)\right\| \leq (1-\beta)\left\|\mathbf{x}'_t - \mathcal{P}_{\mathbf{C}}(\mathbf{x}'_t)\right\| = (1-\beta)\,\text{dist}(\mathbf{x}'_t, \mathbf{C}),$$

where $\mathbf{x}_{t+1} = \mathcal{P}_{\mathbf{C}}(\mathbf{x}'_t)$ is the data-space projection produced by the algorithm.

Because $\mathcal{D}$ is ℓ-Lipschitz we have

$$\text{dist}(\mathbf{x}'_t, \mathbf{C}) = \text{dist}\big(\mathcal{D}(\mathbf{z}'_t), \mathbf{C}\big) \leq \ell\,\text{dist}\big(\mathbf{z}'_t, \mathcal{D}^{-1}(\mathbf{C})\big),$$

where the inverse image is $\mathcal{D}^{-1}(\mathbf{C}) = \{\mathbf{z} : g(\mathcal{D}(\mathbf{z})) = \mathbf{0}\}$. Using the same prox-regularity argument (now applied to the level set of $g \circ \mathcal{D}$), Thus, by the chain-rule and prox-regularity:

$$\|\nabla(g \circ \mathcal{D})(\mathbf{z}) - \nabla(g \circ \mathcal{D})(\mathbf{z}')\| \leq \ell L \|\mathbf{z} - \mathbf{z}'\|,$$

which shows that for a projection in latent space, the contraction factor $(1 - \beta)$ is replaced with

$$1 - \beta' := 1 - \beta/(\ell L).$$

Therefore, denoting by $\mathbf{z}'_{t+1}$ the latent iterate after one full update but *before* decoding, we obtain the fundamental recursion

$$\boxed{\operatorname{dist}\big(\mathcal{D}(\mathbf{z}'_t), \mathbf{C}\big)^2 \;\leq\; (1 - 2\beta'\gamma_{t+1}) \operatorname{dist}\big(\mathcal{D}(\mathbf{z}'_{t+1}), \mathbf{C}\big)^2 + \gamma_{t+1}^2 G^2,} \qquad \text{(non-asymptotic feasibility)}$$

where G is the same (finite) uniform bound used in Part 1. □

H.3 Proof of Theorem 4.2: Fidelity

Proof. Finally, we prove the fidelity bound:

$$\boxed{\mathrm{KL}\big(q(\mathbf{z}_{t-1}) \,\|\, p_{\mathrm{data}}\big) \leq \mathrm{KL}\big(q(\mathbf{z}_t) \| p_{\mathrm{data}}\big) + \gamma_t G^2}$$

We begin by assuming feasibility of the training set $p_{\mathrm{data}} \subseteq \mathbf{C}$. Provided this holds, but the data-processing inequality,

$$\begin{aligned} \mathrm{KL}\big(q(\mathbf{z}_{t-1}) \,\|\, p_{\mathrm{data}}\big) &= \mathrm{KL}\big(\mathcal{P}_{\mathbf{C}}(q(\mathbf{z}'_t)) \,\|\, \mathcal{P}_{\mathbf{C}}(p_{\mathrm{data}})\big) \\ &= \mathrm{KL}\big(\mathcal{P}_{\mathbf{C}}(q(\mathbf{z}'_t)) \,\|\, p_{\mathrm{data}}\big) \\ &\leq \mathrm{KL}\big(q(\mathbf{z}'_t) \,\|\, p_{\mathrm{data}}\big) \end{aligned}$$

This result shows that since the projection operator is a deterministic, measurable mapping, the KL will not be increased by this operation *iff* the training set is a subset of the constraint set (all samples in the distribution fall in $\mathbf{C}$). Hence, subsequently we will ignore the presence of this operator in obtaining our bound.

Next, consider that while in continuous time the application of the true score results in a strictly monotonically decreasing KL, Euler discretizations introduce a bounded error.

Consider that $\mathbf{z}'_t = \mathbf{z}_t + \gamma_t s_t$. Each denoising step shifts the vector $\mathbf{z}_t$ by a vector norm of at most $\gamma_t G$, provided that $\|s_t\| \leq G$.

Lemma H.4. *Suppose $\|s_t\| \leq G$ everywhere, Then,*

$$\mathrm{KL}\big(q(\mathbf{z}'_t) \,\|\, p_{\mathrm{data}}\big) - \mathrm{KL}\big(q(\mathbf{z}_t) \,\|\, p_{\mathrm{data}}\big) \leq \gamma_t G^2.$$

Proof of Lemma H.4.

$$\mathrm{KL}\big(q(\mathbf{z}_t) \,\|\, p_{\mathrm{data}}\big) = \int q(\mathbf{z}_t) \log \frac{q(\mathbf{z}_t)}{p_{\mathrm{data}}} dx,$$

and

$$\mathrm{KL}\big(q(\mathbf{z}'_t) \,\|\, p_{\mathrm{data}}\big) = \int q(\mathbf{z}'_t) \log \frac{q(\mathbf{z}'_t)}{p_{\mathrm{data}}} dx,$$

Therefore,

$$\mathrm{KL}\big(q(\mathbf{z}'_t) \,\|\, p_{\mathrm{data}}\big) - \mathrm{KL}\big(q(\mathbf{z}_t) \,\|\, p_{\mathrm{data}}\big) = \int q(\mathbf{z}_t) \left[\log q(\mathbf{z}_t) - \log q(\mathbf{z}_t + \gamma_t s_t)\right] dx,$$

Since $\|s_t\| \leq G$, we assume that the true score is bounded by a comparable norm $\|\nabla \log p(\mathbf{z}_t)\| \leq G$. A one-step Taylor bound gives:

$$\log p(\mathbf{z}_t) - \log p(\mathbf{z}_t + \gamma_t s_t) \leq \|\gamma_t s_t\| \cdot \|\nabla \log p(\xi)\| \leq \gamma_t G^2$$

for some ξ on the line segment between $\mathbf{z}_t$ and $\mathbf{z}'_t$. Integrating over $q(\mathbf{z_t})$ gives

$$\boxed{\mathrm{KL}\big(q(\mathbf{z}'_t) \,\|\, p_{\mathrm{data}}\big) - \mathrm{KL}\big(q(\mathbf{z}_t) \,\|\, p_{\mathrm{data}}\big) \leq \gamma_t G^2}$$

□

Lemma H.4 can then be directly applied to derive our bound:

$$\boxed{\mathrm{KL}\big(q(\mathbf{z}_{t-1}) \,\|\, p_{\mathrm{data}}\big) \leq \mathrm{KL}\big(q(\mathbf{z}_t) \| p_{\mathrm{data}}\big) + \gamma_t G^2}$$

□